



ISLAMIC UNIVERSITY OF TECHNOLOGY
ORGANIZATION OF ISLAMIC COOPERATION



Experimental study on acoustic energy harvesting using single and double PZT film configuration in Helmholtz resonator

A THESIS SUBMITTED TO THE ACADEMIC FACULTY IN PARTIAL FULFILLMENT OF THE
REQUIREMENT FOR THE DEGREE OF

BACHELOR OF SCIENCE

IN

MECHANICAL ENGINEERING

AUTHORED BY,

A.N.M Nihaj Uddin Shan
Student ID: 160011066

Md. Zayed Mostafa
Student ID: 160011022

MD. IFTEKHAR UDDIN SHOHAN
Student ID: 160011001

Supervised By

Prof. Dr. Md. Anayet Ullah Patwari
Head, Department of Mechanical and Production Engineering (MPE)
Islamic University of Technology
Board Bazar, Gazipur
Dhaka, Bangladesh.

DEPARTMENT OF MECHANICAL AND PRODUCTION ENGINEERING
ISLAMIC UNIVERSITY OF TECHNOLOGY (IUT)

March 2021

CANDIDATE'S DECLARATION

It is hereby declared that their thesis or any part of it has not been submitted elsewhere for the award of any degree or diploma.

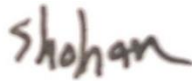
Signature of Candidates



A.N.M Nihaj Uddin Shan



Md. Zayed Mostafa



MD. IFTEKHAR UDDIN SHOHAN

Department of Mechanical and Production Engineering

Islamic University of Technology (IUT)

Board Bazar, Gazipur

Dhaka, Bangladesh

Signature of Supervisor



Prof. Dr. Md. Anayet Ullah Patwari

Head, Department of Mechanical and Production Engineering (MPE)

Islamic University of Technology

Board Bazar, Gazipur

Dhaka, Bangladesh.

CERTIFICATE OF RESEARCH

The thesis title “**Experimental study on acoustic energy harvesting using single and double PZT film configuration in Helmholtz resonator**” submitted by has been accepted as satisfactory in partial fulfillment of the requirement for the degree of Bachelor of Science in Mechanical Engineering on March 2021.

Supervisor



Prof. Dr. Md. Anayet Ullah Patwari

Head, Department of Mechanical and Production Engineering (MPE)

Islamic University of Technology

Board Bazar, Gazipur

Dhaka, Bangladesh.

ACKNOWLEDGEMENT

First of all, this research would not have been completed without the blessings of Almighty Allah for granting us this opportunity to do our bachelor's degree at Islamic University of Technology (IUT).

We want to express our sincere gratitude to our supervisor Dr. Md. Anayet Ullah Patwari, Professor, Department of Mechanical and Production Engineering (MPE), Islamic University of Technology (IUT) for his constant supervision, guidance, support, and motivation throughout our research stages. We are deeply thankful for his invaluable input, advice, and knowledge.

We also would like to thank the Mechanical and Production Engineering Department for providing us with the equipped laboratory to run our experiments. Also, special thanks to Engr. Rakibul Hassan for his great assistance during our experiments.

We also want to extend our sincere appreciation to the staff at the fabrication laboratory of DUET for providing us with the necessary equipment and for their massive help.

Also, we would like to thank our family for their love and support throughout our entire life and our friends for their support and good times. This thesis would not have been possible without them.

Abstract

Acoustic energy harvesting has been the main attraction for many researchers because of energy scarcity. Low-frequency energy harvesting is a highly complicated process. However, the physical characteristics of piezoelectric materials can be utilized to extract energy from low-frequency acoustic or vibration-based waves. In this study, experiments have been conducted on acoustic energy harvesting from low-frequency sound sources using Helmholtz resonator with single and double PZT film configurations. Based on the results obtained from the experiment it is clear that double film configuration is better for the purpose. Under the condition of 100Hz constant frequency single film configuration has been able to give 80.2 mV whereas for double film configuration the value of output voltage was 237.6 mV. A rectifying circuit was simulated using commercial software which is run by the output of the noise barrier. The noise barrier of the double film configuration can produce a total power of 268.8 mW where one film configuration has a total power output of 136.77 mW. Modified Helmholtz resonator noise barrier of double film configuration can be used to power up low power-consuming devices and greatly applicable for noise reduction in big cities and industrial areas.

Keywords

Acoustic energy harvesting; Cantilever beam; Helmholtz Resonator; PZT film; Metro rail; Noise barrier.

Table of Contents

Abstract	Error! Bookmark not defined.
List of Figures	viii
List of Tables	x
Chapter 1: Introduction	11
1.1. Introduction	11
1.2. Objectives	13
1.3. Thesis Organization	13
Chapter 2: Literature review	14
2.1. Literature review	14
2.2. Acoustic energy harvesting mechanism	18
Chapter 3: Research Methodology	19
3.1. Methodology	19
3.1.1. Helmholtz resonator and theoretical model	19
3.1.2. Bending of a single-layer piezoelectric cantilever under dynamic pressure	21
3.2. Geometry	25
3.2.1 Single Unit of Helmholtz Resonator	26
3.2.2. Array Design	29
3.3. 3D Printing Machine	31
3.3.1. 3D Model	32
3.4. PZT film description	35
3.5. Experimental details	37
3.5.1. Components description	37
3.6. Experimental setup	41
3.7. Boundary Condition	42

3.8. Rectifying circuit simulation	43
Chapter 4: Results and Discussions	46
4.1. Experimental results	46
4.2. Simulation results	53
Chapter 5: Future scope and Conclusion	57
References	58

List of Figures

Figure 1. The architecture of the study.	12
Figure 2. Power density vs. voltage[27].	18
Figure 3. Schematic diagram of a Helmholtz resonator and its inside mechanics.	20
Figure 4. Theoretical diagram of the resonator.	20
Figure 5. (a) The cross-sectional view of a multi-layer piezoelectric cantilever and (b) the equivalent electric circuit diagram of a multilayer piezoelectric generator. The arrows of each piezoelectric layer indicate the polarization direction induced by beam bending. [35]	21
Figure 6. The base of the resonator.	26
Figure 7. The outer boundary of the prototype.	27
Figure 8. Cross-section view of the prototype (1 film)	27
Figure 9. Cross-section view of the prototype (2 films).	28
Figure 10. Front view and dimension	29
Figure 11. Bottom view and dimension	29
Figure 12. Top View of the array.	30
Figure 13. Isometric View of array	31
Figure 14. 3D printing machine	32
Figure 15. Top view of the prototype	32
Figure 16. Side view of the prototype	33
Figure 17. Front View of prototype	33
Figure 18. Disassemble View of prototype.	34
Figure 19. PZT film.	35
Figure 20: Function generator	37
Figure 21: Oscilloscope	38
Figure 22: Power amplifier	39
Figure 23: Speaker	40
Figure 24. Experimental Setup	41
Figure 25. Flow diagram of the experimental setup.	42
Figure 26. Rectifying circuit considering the single film configuration.	44
Figure 27. Rectifying circuit considering the double film.	45

<u>Figure 28. Input voltage vs. Output voltage for a single film without the resonator.</u>	47
<u>Figure 29. Frequency vs. Voltage for a single film without the resonator.</u>	48
<u>Figure 30. Input vs. output Voltage at 100 Hz for both single and double film configuration with a resonator.</u>	49
<u>Figure 31. Output voltage vs frequency at 500 mV input voltage for both single and double film configuration with a resonator</u>	50
<u>Figure 32. Output voltage vs frequency at 1000 mV input voltage for both single and double film configuration with a resonator.</u>	51
<u>Figure 33. Output voltage vs sound pressure level for single film configuration.</u>	52
<u>Figure 34. Output voltage vs sound pressure level for single film configuration.</u>	52
<u>Figure 35. Output voltage vs sound pressure level for single and double film configuration.</u>	53
<u>Figure 36. Input and load current vs time plot for one film AEHNB model.</u>	54
<u>Figure 37. Input and load voltage vs time for one film AEHNB model.</u>	54
<u>Figure 38. Input and load current vs time plot for two films AEHNB model.</u>	55
<u>Figure 39. Input and load voltage vs time for two films AEHNB model.</u>	55

List of Tables

<u>Table 1</u>	36
<u>Table 2</u>	36
<u>Table 3</u>	43

Chapter 1: Introduction

1.1. Introduction

Acoustic sound waves are mechanical waves that have energy and can be created by a wide range of noise sources. When the sound wave is unwanted, it's referred to as noise. Aircraft, vehicles, high-speed trains, power stations, loudspeakers, and expressways are the common sources of noise. Now many researchers [1–10] have focused on energy harvesting and they have developed many ways of converting ambient vibration energy in the environment and it transforming into valuable energy in the form of electricity. The expression "energy harvesting" refers to small-scale energy production on the order of micro-to-milli-watts. Theoretically and experimentally, harvesting energy from solar [11], wind [12], biochemical [13], thermal [14], and mechanical vibration [15] has been investigated for driving low-power appliances. However, the least attention has been paid to developing methods of harvesting acoustic energy compared to other energy sources. Acoustic energy is an available, ample, viable, and non-pollution source of energy that can be extracted and converted into electrical energy. Recently, there have been substantial resources to enhance mechanisms to harvest acoustic energy from industries, road traffic, work plants, construction sites, airports, and expressways [10]. Also, the conversion of mechanical vibration (sound) energy to electrical energy can be performed using three types of generator, namely piezoelectric generators, electromagnetic and electrostatic. Amongst these three mechanisms, most consideration has been devoted to piezoelectric transduction. Piezoelectric (PZT) is a sophisticated replacement for batteries that can generate energy on the go. A lot of research has been done on this topic. Horowitz et al. [2] was introduced to the first micromachined acoustic energy harvester using a piezoelectric ring attached to one of the walls of the Helmholtz resonator. At a sound pressure level of 149 dB, he was able to reach a maximum power of $250 \mu\text{Wcm}^{-2}$. Then, based on the same principle, an electromechanical Helmholtz resonator was developed by Fei Liu et al.[16], which bends the piezoelectric plate using the uniform pressure of the sound incident wave in the resonator compartment. At an incident sound pressure level of 160 dB, this study was able to harvest the power of 30 mW which is enough to supply small powered electronic appliances. Kim et al. [14] used the Helmholtz resonator to harvest airflow and

aeroacoustic energy using the magnet driven by the acoustic pressure principle. They achieved a peak-to-peak output voltage of 4 mV at 1.4 kHz where input pressure was 0.2 kPa.

The majority of the studies above produced power/voltage at a high-frequency, which is used in military and government communication systems, aviation, and over-the-horizon radar systems. These types of applications are not seen regularly. As a result, the need for acoustic energy harvest from low frequencies that are present in our daily life, such as traffic, TVs, aircraft, metro rail, industries, and many other sound sources, is discovered and investigated in this work. However, all previous studies produced power using a single piezoelectric beam, and the use of dual piezoelectric beams has not been investigated. As a result, the primary goal of this study is to figure out a new method for extracting energy from low-frequency sound waves that employ dual piezoelectric beams with a honeycomb structure Helmholtz resonator. Due to the use of dual PZTs, this method can double the amount of energy harvested. A honeycomb structure Helmholtz resonator will be fabricated after designing an acceptable PZT setup to amplify the voltage produced by the PZT setup. The architecture of our work is shown with the help of a flowchart in **Figure 1**.

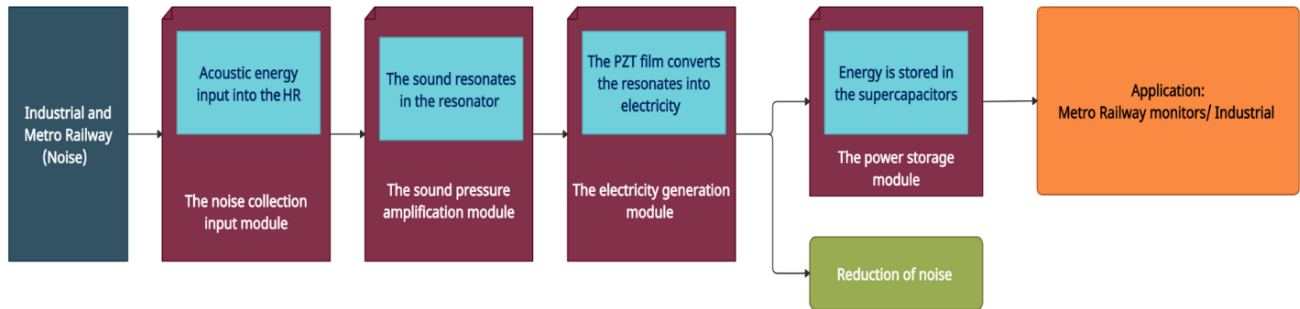


Figure 1. The architecture of the study.

1.2. Objectives

The main objective of the research is to develop the currently existing technologies in the field of acoustic or vibration-based energy harvesting using piezoelectric materials and noise reduction in big city residential and industrial areas. The research methodology has been developed in such a way that the technological advancements related to low-frequency sound energy harvesting can be applied in real life scenarios.

The research purpose was to further develop the acoustic energy harvester unit developed in the study of Wang et al. by increasing the number of piezoelectric film and assessing the potential of easily available piezoelectric material. For this purpose, lead zirconate titanate (PZT) films have been selected. Since the research is done to develop energy harvesters for practical applications, the model is to be developed physically and experimentation on the model has to be done utilizing only low frequency sources.

1.3. Thesis Organization

This study begins with an introduction that provides background information on acoustic energy harvesting, accompanied by a literature review of previous methods for harvesting energy from low frequency sound and vibration sources. In Chapter 2, a detailed literature review of previous studies is briefly discussed, as well as the acoustic energy harvesting mechanism. The design of double cantilever PZTs, as well as the Helmholtz resonator with honeycomb structure, detailed description of our work methodology have been presented in chapter 3. Chapter 3 employs a conventional mathematical approach to model the cantilever PZT. Also, in Chapter 3, an experimental investigation of the cantilever PZT design setup and acoustic energy harvesting noise barrier of our thesis is presented. In Chapter 4, the result and discussion from the experiments are presented to verify the feasibility and advantage of double film noise barrier system over the currently existing single film units. The simulation results of the rectifying circuit for the acoustic energy harvesting unit noise barrier are also presented in Chapter 4. Finally, summary of the findings and suggestions for future studies are given in chapter 5.

Chapter 2: Literature review

2.1. Literature review

Mickaël et al. [6] attempted to increase the power gain in high-frequency acoustic energy harvesting. Zutao et al. [17] proposed a kinetic energy recovery device to capture the energy wasted by vehicles going through a road tunnel. Also, Zhang et al. [18] introduced a new shock absorber to collect the waste of suspension energy from moving vehicles for use in extended electric vehicles. Energy harvesting technologies will be a promising substitute for energy shortages [19]. Orrego et al. [20] developed a novel wind energy harvester by self-sustaining oscillations of a flexible piezoelectric membrane fixed in an inverted orientation. Helios Vocca et al. proposed a vibration harvesting system using bi-stable oscillators to model nonlinear piezoelectric harvesters, to explore the prospective of noise-driven dynamics [21]. Xingtian et al. [22] established a portable electromagnetic energy harvesting design that utilizes mechanical transmission to transform railroad vibrations into electricity, and the proposed energy harvester was found to be efficient in testing, with a 55.5% efficiency. The use of piezoelectric designs to transform vibrational energy to electrical energy has gained a lot of attention in recent years due to their advantages such as high transduction efficiency, simplicity of configuration, and so forth.

Lukai et al. has developed an advanced harvesting pavement device in which piezoelectric asphalt layers become conductive, allowing vehicles' kinetic energy to be harvested. The maximum electrical output can be up to 300 mW. Hossein et al. [23] clarified the suitability of harvesting mechanical energy from vehicle strain and stress produced on highways. They conducted experiments to see whether piezoelectric materials could be used to harvest energy from asphalt pavements. For intermediate appliances, the electromagnetic transducer is frequently used in low-frequency ranges. The electromagnetic transducer is consistent with Si microsystems technology to a good extent [24]. It can also run at a higher frequency (50 Hz), resulting in a higher power density [25].

However, since it is difficult to design and produce, one of the disadvantages is the high cost of integrating it with a microsystem. Another drawback is the dense size of the permanent magnets and the timing coil. The electrostatic mechanism, which is the best match for MEMS applications

and does not require smart material, is the second mechanism. However, this type of charger involves an external voltage source, such as a battery, and has mechanical limitations. The very last form of a transducer is the piezoelectric transducer, which is very general. This is due to the material properties that make it very alluring, where these materials have a convenient configuration, a high density of power, a high level of single-crystalline coupling and a high degree of viability for daily applications [26]. Vatansever et al. [7] studied the production of renewable energy from raindrops and wind speeds. Ceramic-based piezoelectric fiber composite structures (PFCs) and polymer-based piezoelectric strips, PVDF (Polyvinylidene fluoride), were used to generate voltage from these natural phenomena for use in driving small devices. Conclusions were drawn after running different experiments on both piezoelectric materials and varying parameters such as droplet weight, releasing height and wind speed. The higher the voltage was produced, the greater the height and mass of the water drops. The amount of energy scavenged is determined by the material's geometric dimension and the type of film employed. And then, it was shown that when a polymer-based piezoelectric material was being used in this implementation, the peak voltage became higher than when ceramic piezoelectric materials were being used. After this, additional research into piezoelectric materials and their implementations is carried out. According to Vatansever et al. [7], Li et al. [9] use PZT beams as a piezoelectric material in his tube resonator. To check the output voltage of the piezoelectric material plates, two separate length tube resonators were built. The effects of using two piezoelectric materials, PVDF and PZT, on a 52 cm and 42 cm tube resonator is investigated. When a single PVDF beam was positioned near the open inlet of the 52 cm tube resonator, it produced 0.105 V and 55.6 nW. When a single beam became mounted, the 42 cm tube produced voltage and power density of 1.433 V and 0.193 mW, respectively. As 5 to 7 PVDF beams were mounted in the 52 cm tube, the output voltage and power became increased to 0.42V and 171.48 nW at 100 dB, respectively. As 4 to 6 beams were mounted in the 42 cm tube, the PZT showed 9 and 1813 times higher voltage and power rises than the PVDF (3.789 V and 0.311 mW, respectively). Subsequently, they harvested a low frequency traveling sound within a tube resonator of 42 cm which is open from a single end and contains titanium plates (PZT). When the incident moving sound frequency matches the resonator resonance frequency, the increased acoustic pressure within the tube excites the piezoelectric plates' vibration motion, allowing voltage generation. For the first eigenfrequency (199 Hz), the amplification factor was 97.2. Once the incident sound pressure was increased to 110 dB, the voltage generated

raised to 15.689 V, suggesting that the voltage and incident sound pressure have a linear relationship. The corresponding power is 12,697 mW and the area (power per unit area) and the volume power densities are 0,635 mW cm⁻² and 15,115 μW cm⁻³, respectively [10]. Then, using commercial finite element software (COMSOL software, they were able to simulate the quarter-wavelength resonator based on the same result of [27]. At the first eigenfrequency (198 Hz), the simulated model had an amplification factor of 100.1, while the experimental model had an amplification factor of 97.2. A single PZT produced 1.6 V at 196 Hz when simulated at 100 dB. When compared to the experimental data, it produced 1.43 V at 199 Hz, which was similar. The PZT plates were then increased to 4 PZT and generated 0.37 mW at 190 Hz. Following that, the beams were increased to 5 PZT plates, generating 4.06 V at 189 Hz. It can be assumed that the experimental data (3.79 V at 193 Hz and 0.31 mW at 194 Hz) [28] was 7% and 19% lower than the results of the simulation. Afterward, Li et al. [8] used PVDF cantilever beams to monitor the 58 cm tube resonator in two different configurations: aligned and zigzag. In comparison to the aligned design, the zigzag structure showed a substantial increase in voltage and power. The zigzag configuration provides a wider path for acoustic air particle motion, resulting in a higher amplification ratio. The amplification ratios for the first three eigenfrequencies, 146 Hz, 439 Hz, and 734 Hz, are 59.1, 42.2, and 23.3, respectively. When several PVDF beams have been used, the maximum voltage is 0.696 and the current is 0.31 μW at 100 dB. And due to the linear connection between SPL and output voltage, when the pressure level reached 110 dB, the voltage increased to 1.35 V [9]. Abdelmoula et al. [29] studied a low-frequency Zigzag energy harvester with torsion bending properties and confirmed that the proposed torsion-dominant mode provided a higher harvested power level while lowering the operating frequency by half. Guan et al. [30] developed a piezoelectric system for gaining rotational energy, for example, generators built into the interior surface of tires of the vehicle. The frequent deformations of the piezoelectric elements are transported to electricity while the energy collector rotates, at rotating frequencies of 7–13,5 Hz an output power of 83.5–825 μW is gained [30]. Despite comprehensive research into various energy resource harvesting technologies, there are still untapped and unused energies all around us. For example, acoustic energy is a significant energy resource that is relentlessly produced but stays unused [9]. Sound waves are pressures that spread in elastic media. Sound waves. In an environment, acoustic energy can be obtained. Acoustic energy harvesting (AEH), which transforms environmental acoustic waves into electricity using a resonator or a transducer, has

now become viable with the fast technological development of autonomous microelectromechanical systems (MEMS) [31].

Zhiyong et al. [32] demonstrated an acoustic energy harvester in a bistable state with a flat plate that is excited to vibrate, and when reaching a coherence resonance, a high voltage output was produced for a specific sound pressure level (SPL). In general, an acoustic resonator is used to enhance the sound pressure in an acoustic field at a particular frequency band in addition to absorbing an unwanted frequency element of a sound system [31]. Helmholtz resonators (HRs) are one of the most widely employed acoustic resonators as a noise-controlling system [33].

Liu et al. [16] investigated the development of an acoustic energy harvesting system based on an electro-mechanical Helmholtz resonator (EMHR), which usually consists of a cavity, orifice, and piezoelectric diaphragm. In the case of an incident SPL of approximately 160 dB, the power output can be up to nearly 30mW, which is sufficient to power many low-power electrical appliances [16]. Due to the low sound strength, Yuan et al. [34] suggested focusing on increasing the output power of acoustic energy gathering and introduced a unique design for harvesting acoustic energy. The suggested high device is primarily made up of an HR with an unfixed bottom that works well with low-frequency sound waves. Kim et al. [14] constructed an acoustic energy scavenger for the use of large amplitude acoustic waves, which formed in response to the air flowing through the entrance of the HR. Noh et al. [35] suggested a piezoelectric cantilever incorporated into the HR. To enhance the efficiency of harvesting energy, the mechanical resonance of the piezoelectric cantilever was consistent with the acoustic resonance of the HR. Although existing initiatives have partially addressed the problems of noise pollution and energy waste, some aspects of (MR/Industries/Airport) noise have not yet been resolved. Two key technological facts remain a challenge for researchers: (1) Noise insulation and absorption have been highlighted, but the harvesting of noise energy to power small electronic devices is ignored in (MR/Industries/Airport). (2) The popularity of (MR/Industries/Airport) requires higher effectiveness of noise barriers for noise removal, especially for low-frequency noise that mostly manages to escape established noise barriers along (MR/Industries/Airport).

To follow up on and resolve the aforementioned concerns, we suggested in this paper a noise barrier for (MR/Industries/Airport) that harvests alternative acoustic energy using an HR and a PZT film to achieve both electricity generation and noise reduction. Supercapacitors are used in

an energy storage unit to power some small electronic devices and deliver as reserve power supplies along (MR/Industries/Airport), such as runway lights of the airport, metro rail monitors, small electronic appliances of industry, and maintenance.

2.2. Acoustic energy harvesting mechanism

Energy harvesting, especially vibration-based energy, has received a lot of attention in the last decade. Many methods for extracting vibrational energy and transforming it into electricity for microsystems have been developed by researchers [36].

In comparison to other transductions, the piezoelectric material can withstand a large amount of strain to transform mechanical energy into electrical energy. **Figure 2** illustrates the piezoelectric's high power density as a function of voltage, as opposed to other mechanisms.

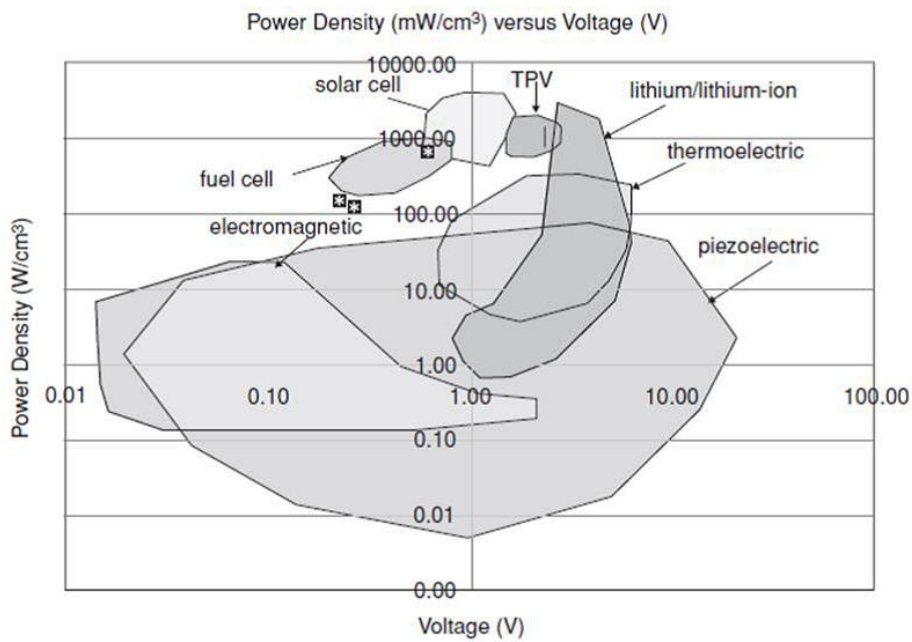


Figure 2. Power density vs. voltage[27].

Chapter 3: Research Methodology

3.1. Methodology

The methodology generally expresses the step-by-step work done in this experiment. The theory behind this experiment was spring-mass and beam theory. The theory expressed how the system will act when the experiment will run. Then the model design of the prototype comes into the next phase. Then the CAD file will be converted into the 3D model by which the experiment will be done. After that experimental setup will be arranged with various components. Like function generator, power amplifier, oscilloscope, speaker, etc. Array and the rectifying circuit were also developed to expand our future work.

3.1.1. Helmholtz resonator and theoretical model

If the sound pressure level of incident sound in a normal environment is 100 dB then it is seen that the sound pressure is as low as 2 Pa which creates very minimal excitation on the piezoelectric film. The whole science around sound energy harvesting works with very low-quality waste energy extraction which is mostly in the dissipated form in the surrounding environment. Technological advancements in the field of sound energy have brought different kinds of resonator structures. application of the Helmholtz resonator is very commonly seen in engine mufflers. The transmission characteristics, loss, acoustic behavior and sound pressure level when observed for these resonators depicts the amplification of incident sound impedance on the film providing better excitation [28]. The Helmholtz resonator consists of a neck and a cavity. The cavity is generally very large compared to the inlet and neck. The walls of the body are assumed to be a sound hard boundary. The acoustic system of the Helmholtz resonator is equivalent to a single degree of freedom spring-damper system for the lower mode. A schematic diagram of a Helmholtz resonator is shown in **Figure 3** along with the equivalent spring-mass and damper model.

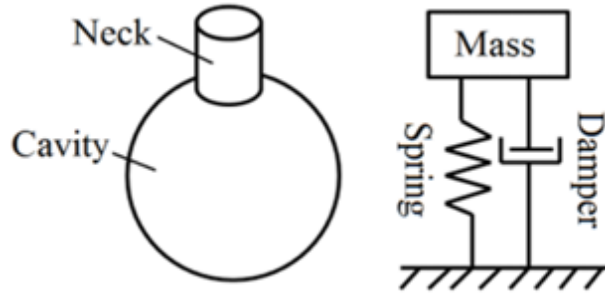


Figure 3. Schematic diagram of a Helmholtz resonator and its inside mechanics.

The single degree of freedom system ensures that the sound pressure is significantly amplified inside the cavity at a definite frequency, which means that acoustic resonance is taking place hence the name resonator. According to the lumped element method, its fundamental acoustic resonant frequency can be calculated considering c is the sound speed, S is the neck's cross-sectional area, L is the neck length, V is the cavity volume, a is the radius of the open neck.

$$f = \frac{c}{2\pi} \sqrt{\frac{S}{LV}} \quad (1)$$

The air in the neck oscillates and acts as the mass of the single degree of freedom system, and the air inside the cavity expands and contracts like a spring. The damping in the system is achieved by the viscous losses due to the friction of the oscillating air in the neck and the radiation losses at the end of the neck [37]. The resonant frequency depends on the size of the cavity and the connection tube.

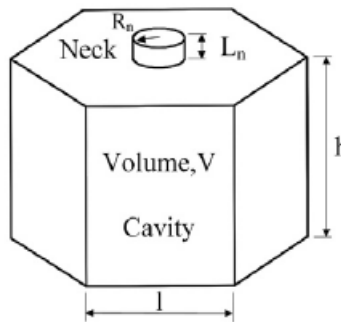


Figure 4. Theoretical diagram of the resonator.

The Helmholtz resonator used in this study is hexagonal shaped to maximize the surface area usage in the acoustic energy harvester units (AEHU). The theoretical model is depicted in **Figure 4** and

the acoustic behavior is similar to any Helmholtz resonator. As shown in **Figure 5** the hexagon shape helps to arrange these resonators together in a beehive-like structure. In the study conducted by Wang et al. acoustic energy harvester noise barrier (AEHNB) has shown success in sound energy harvesting [our main paper]. Hence, a hexagonal resonator has been chosen for this study. Here R_n is the radius of the neck which will give us the total surface area of the neck. The length of each side of the hexagon is l and the height of the resonator cavity is h which in turn gives the volume of the cavity V .

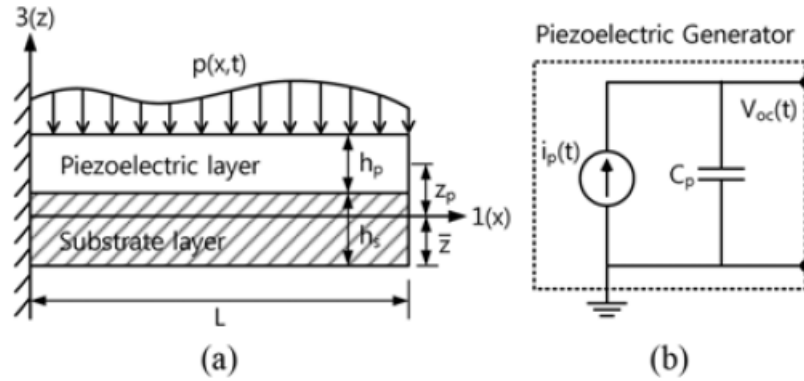


Figure 5. (a) The cross-sectional view of a multi-layer piezoelectric cantilever and (b) the equivalent electric circuit diagram of a multilayer piezoelectric generator. The arrows of each piezoelectric layer indicate the polarization direction induced by beam bending. [35]

3.1.2. Bending of a single-layer piezoelectric cantilever under dynamic pressure

An AC electric field and an external excitation force, or both, can be used to move a single-layer piezoelectric composite cantilever into lateral vibration, as shown in **Figure 5(a)**. As a result of the beam's bending deflection, strains along the x-axis and current across the electrodes are induced. As a result, the piezoelectric constitutive equations are based on the fact that the piezoelectric phase operates as a 31-mode operation in the current configuration [36,37].

$$S_1 = s_{11p}^E T_1 + d_{31} E_3 \quad (3)$$

$$D_3 = d_{31} T_1 + \epsilon_{33}^T E_3$$

where, T_1 and S_1 are the stress and strain in the length direction of a piezoelectric layer, respectively; D_3 and E_3 are the electric field and electric displacement, respectively; s_{11p}^E , ϵ_{33}^T ,

and d_{31} , are the elastic compliance at the constant electric field, the permittivity at a constant stress of the piezoelectric layer, and the transverse piezoelectric coefficient, respectively.

In this investigation, axial strains of all layers associated with bending displacement, $S_x (=S_I) = -z (\partial^2 w / \partial x^2)$, caused by an external harmonic loading are only considered and assumed to be the same. When a distributed external force is applied to the piezoelectric cantilever bilayer shown in Fig. 2(a), the beam motion equation for an undamped lateral vibration modeled using the standard Euler-Bernoulli beam theory is given as [40]

$$D \frac{\partial^4 w(x,t)}{\partial x^4} - m_t \frac{\partial^2 w(x,t)}{\partial t^2} = p(x,t) \quad (4)$$

where $w(x, t)$ is the lateral deflection of the beam, D is the global flexural rigidity of the bilayer composite, $p(x, t)$ is a distributed external force per unit length of the beam, and m_t is the total mass per unit surface of a cross-section of the composite beam. The global flexural rigidity and the total mass per unit surface of a cross-section of the single-layer composite is given by

$$D = \frac{h_p}{12s_{11p}^E} \{h_p^2 + 3[h_p + 2(h_s - \bar{z})]^2\} + \frac{h_s}{12} E_{Ys} \{h_s^2 + 3(h_s - 2\bar{z})^2\} \quad (5)$$

$$m_t = \rho_s h_s + \rho_p h_p,$$

where h_s and h_p are the thickness of the substrate and piezoelectric material, respectively, ρ_s and ρ_p are the density of substrate and piezoelectric layer, E_{Ys} is the elastic constant of the substrate, respectively, and \bar{z} is the distance from the neutral plane to the bottom surface of the beam given by

$$\bar{z} = \frac{E_{Ys} h_s + s_{11p}^E h_p^2 + 2s_{11p}^E h_p h_s}{2(s_{11p}^E h_p + E_{Ys} h_s)}$$

For a uniformly distributed harmonic loading condition, $p(x, t) = p(t) = p_0 \cos(\omega t)$, the beam deflection can be the form, $w(x, t) = W(x) \cos(\omega t)$, and substituting this possible solution into equation and further simplifying equation (4) with $k^4 = m_t \omega^2 / D$ and $q_0 = p_0 / D$ leads to

$$\frac{d^4 W(x)}{dx^4} - k^4 W(x) = q_0, \quad (6)$$

where $W(x)$ is the overall mode shape of the beam, ω is the angular frequency, k is the flexural wave number, and p_0 is the amplitude of the uniform pressure. As a result, the solution of this inhomogeneous equation, Equation, can be written as[38]

$$W(x) = c_1 \sin(kx) + c_2 \cos(kx) + c_3 \sinh(kx) + c_4 \cosh(kx) - \frac{p_0}{Dk^4} \quad (7)$$

The constants c_1 , c_2 , c_3 , and c_4 are calculated using the cantilever beam's boundary conditions, which are as follows;

$$W(0) = \frac{dW(x)}{dx} \Big|_{x=0} = \frac{d^2W(x)}{dx^2} \Big|_{x=L} = \frac{d^3W(x)}{dx^3} \Big|_{x=L} = 0. \quad (8)$$

As a consequence of the above boundary conditions, the constants obtained are

$$\begin{aligned} C_1 (= -c_3) &= \frac{W_0 [\sin(kL) \cosh(kL) + \cos(kL) \sinh(kL)]}{2[1 + \cos(kL) \cosh(kL)]}, \\ C_2 &= \frac{W_0 [1 + \cos(kL) \cosh(kL) - \sin(kL) \sinh(kL)]}{2[1 + \cos(kL) \cosh(kL)]}, \\ C_3 &= \frac{W_0 [1 + \sin(kL) \sinh(kL) + \cos(kL) \cosh(kL)]}{2[1 + \cos(kL) \cosh(kL)]}, \end{aligned}$$

where $W_0 = p_0/Dk^4$.

The generated electric charge, $Q(t) = Q_p \sin(\omega t)$, due to uniform pressure harmonic loading in the bilayer piezoelectric cantilever can be determined by integration of D_3 in Equation (3) over the electrode surface and thus the amplitude of $Q(t)$ is expressed as

$$\begin{aligned} Q_p &= b \int_0^L D_3 dx \\ &= \frac{z_p d_{31} b}{s_{11}^E} k W_0 \left[\frac{\sin(kL) - \sinh(kL)}{1 + \cos(kL) \cosh(kL)} \right] + C_0 V, \end{aligned} \quad (9)$$

where z_p is the distance from the neutral plane to the middle of the piezoelectric layer thickness, b is the width of a bilayer cantilever, C_0 is the capacitance given by $C_0 = \epsilon_{33}^T b L / h_p$ of the piezoelectric layer and V is the potential of the piezoelectric material. Correspondingly the induced current, $i_p(t) = I_p \cos(\omega t)$ and the open-circuit voltage, $V_{oc}(t)$, for harmonic excitation can be obtained from Equation (9) as

$$I_p = \left| \frac{dQ(t)}{dt} \right| = \omega Q_p = \omega (\gamma_p p_0 + C_0 V)$$

(10)

$$|V_{oc}(t)| = Kp_0$$

where γ_p , the coupling factor between the induced electric charge and the applied pressure, and K , the open-circuit voltage sensitivity, are given by

$$\gamma_p = \frac{z_p d_{31} b}{D k^3 s_{11p}^E} \left[\frac{\sin(kL) - \sinh(kL)}{1 + \cos(kL) \cosh(kL)} \right] \quad (11)$$

$$K = \frac{z_p d_{31} h_p}{D k^3 s_{11p}^E \epsilon_{33}^T L} \left[\frac{\sin(kL) - \sinh(kL)}{1 + \cos(kL) \cosh(kL)} \right]$$

According to Equation (10) and Equation (11), the open-circuit voltage of the single-layer piezoelectric cantilever excited by a uniform pressure is proportional to the amplitude of the applied pressure, p_0 , along with the open-circuit voltage sensitivity, K . Moreover, the expression of Equation (10) can be represented by the equivalent electric circuit consisted of a current source and a parallel-connected capacitor shown in **Figure 5(b)**.

Now, the final expression of the amplitude of induced current and open-circuit voltage by an amplified acoustic pressure through Helmholtz resonator can be obtained by substituting Equation (1) into Equation (10) as

$$I_p = \omega(\gamma_p G p_i + C_0 V) \quad (12)$$

$$|V_{oc}| = K G p_i$$

where p_i is the external driving pressure amplitude of the incident sound wave and G is the pressure amplification factor of the resonator at its resonance frequency. The resonance of the vibrating beam occurs when the denominator of the displacement, Equation (7), is equal to zero and thus the resonance frequencies are given by

$$f_n = \frac{(kL)_n^2}{2\pi L^2} \sqrt{\frac{D}{m_t}}, \quad (13)$$

where the first three values of $(kL)_n$ are $(kL)_1 = 1.875$, $(kL)_2 = 4.694$, $(kL)_3 = 7.855$. Consequently, it is needed to adjust the resonance frequencies of the piezoelectric composite cantilever in

Equation and the acoustic resonator in equation (1) to be the same to attain the maximum producing power.

3.2. Geometry

In this section of the paper, it will be discussed that what is the process to make the prototype model for the experiment. For creating this prototype various process was there. The main prototype was to build in the simplest way. SolidWorks (2020) was used here to creating the prototype. The main challenge was there to build the inner part of this model. As it is so much complicated to deigned the part which contained the PZT film. The distribution of the weight of the PZT film was one of the main problems. this problem was solved accordingly by applying various operations and other calculations. After that, there was some problem in the outer design too. There was also another problem to watch. As it was going to creating by a 3D printing machine the model has to be so simple to create

There are two sections of geometry to analyze. Two of the geometry are important for this experimental work process.

1. Single Unit of Helmholtz Resonator

2. Array Design of Helmholtz Resonator

For the experiment, a single unit of the Helmholtz Resonator was used. For creating the model there was so much operation to be conducted. The operations are the key part to make the model. Some complication was there. Like how to design the piezoelectric material and how to give the impedance on the positive portion of the film. One of the main problems was to achieving the optimized model. By which the experiment can fully be conducted. As the optimized here refer to the main layout of the model. Meaning what might be the best dimension for the model and what kind of material to be used. To achieve the best combination trial and error process has been done accordingly. A fully specified and effective model has been created accordingly. The HR has a hexagonal shape on it. Hexagonal shapes are the most optimized shape as the maximum hexagonal shape can be fit in one certain area. So here we prefer this shape. There were lots of other shapes to be count. But achieving the best structure hexagonal shape was the most accurate one. There is a noise barrier which will be discussed lately where is concept will come much clear.

3.2.1 Single Unit of Helmholtz Resonator

For creating the CAD model SolidWorks was used. It was created in a trial-and-error process to achieve the most optimized model. Modified Helmholtz Resonator design was shown [41]. CAD design was focused on how many films will be used. One film concept was already developed [41]. But it was also developed that more than one film can be used for better results. For that purpose, another CAD model was developed where 2 films were used. For creating that model, the various outcome was there. But the better model was picked based on simplicity and effective performance. As the 3D printing of that model has to be made. So, the simple model was chosen.

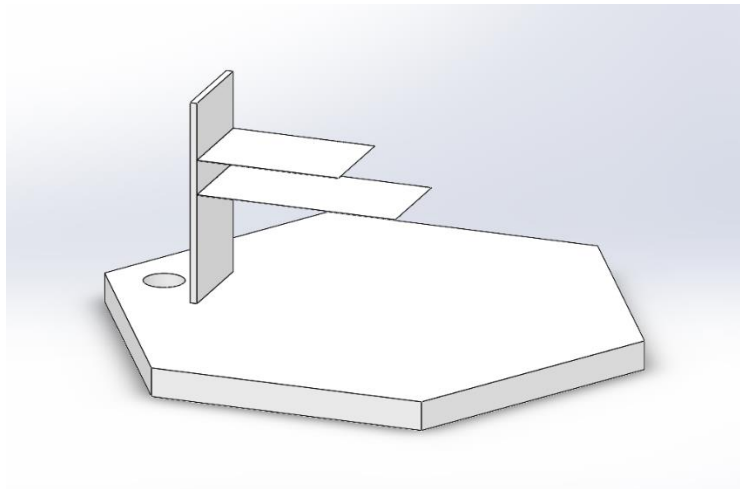


Figure 6. The base of the resonator.

Firstly the base of the prototype was designed. It was also the inner part of the prototype which contained the PZT film. As the PZT film was an important part of the prototype so it has to be designed accordingly. On the other hand, there was a hole in the bottom part of the model. Which was included to make the pass for the cord of the PZT films.

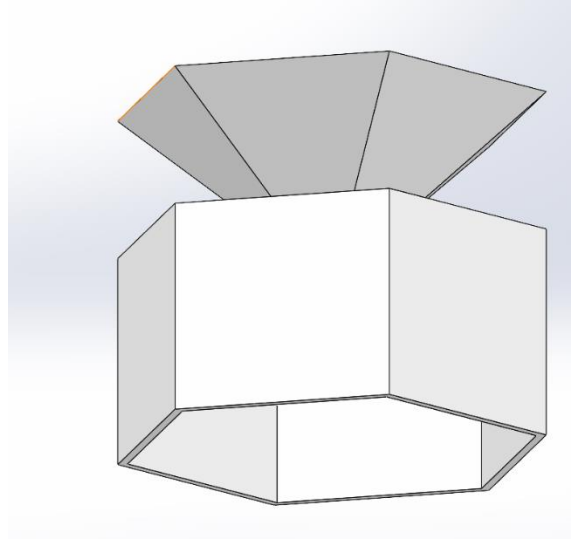


Figure 7. The outer boundary of the prototype.

The outer part of the prototype has a hexagonal shape on it. And the top part also has that shape. The main reason for having that hexagonal shape because that kind of shape can be fit into any kind of barrier. And will have the maximum amount of HR to be fit into a certain area. The sound will go through the top part. For this, the design is done accordingly. The radius of the top part has to be accurate to maintain the sound signal which will go into the piezoelectric material. The outer part also has to be less thick. As it will be placed in various places to extract the sound energy. So the outer part has to be defined accordingly which the condition demands.

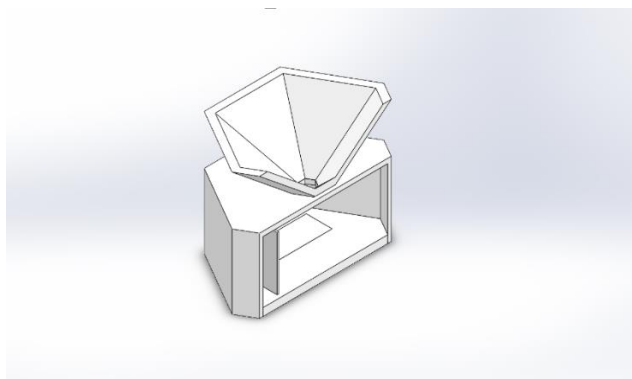


Figure 8. Cross-section view of the prototype (1 film)

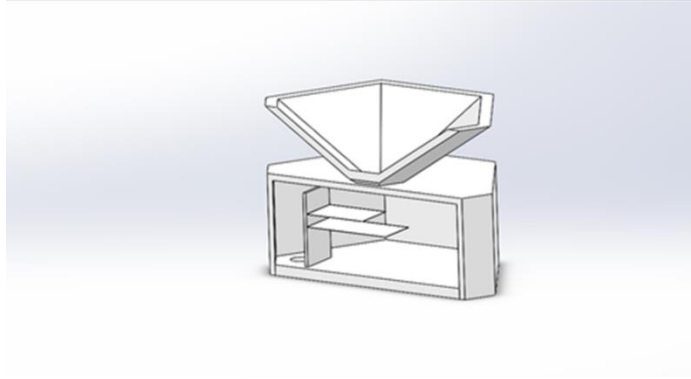


Figure 9. Cross-section view of the prototype (2 films).

Firstly one film model was created to experiment with the voltage output of the system. And to validate the work of another research [41]. For that, this model was designed. The prototype was created by doing the assembly operation in SolidWorks. After that experimental work was done with that. And the desired output was found. The one film concept for this prototype got into the two film concepts which was the main work behind all the work. A low-frequency sound wave was capture by the top part. So its have to be a sophisticated design. The cross-section views the internal as well as the outer part of the prototype.

Here it represents the two film prototypes. The main experiment was done by it. All setup was the same as one film setup. Here also low-frequency sound waves have to be capture. And the results are discussed in the results and discussion chapter. Hexagonal-shaped outer boundary nad and top part also the part of this prototype. Only the main difference is here it is developed with two films one the other hand previous one only having one film. This prototype was the main design for our experimental setup. 3D printing of this model was used for the experiment. The cross-section views the internal as well as the outer part of the prototype.

The dimension of the prototype was given in **Figure 10** and **Figure 11**. Dimension was chosen by trial and error process to obtain the better possible model.

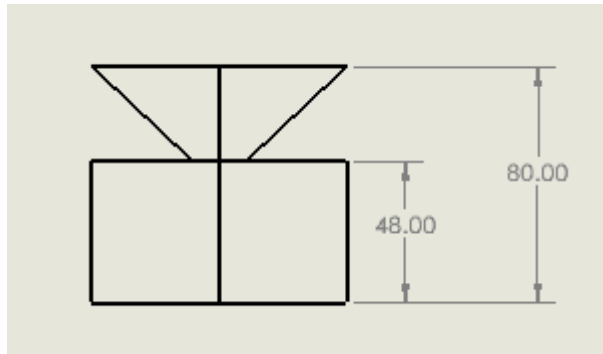


Figure 10. Front view and dimension

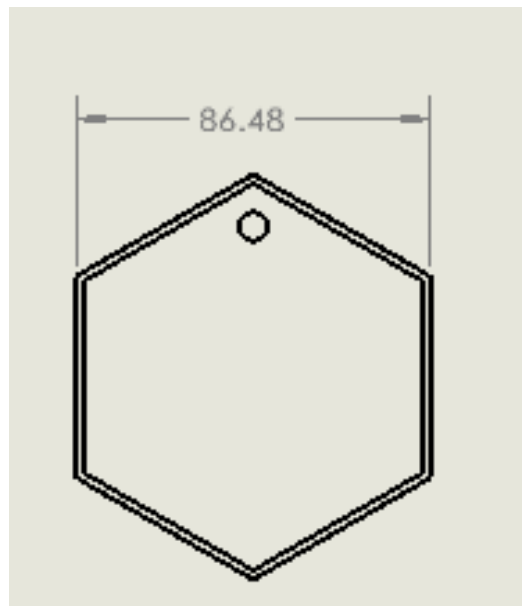


Figure 11. Bottom view and dimension

In **Figure 10** the front view of the model. And the length of the prototype. And there is the bottom view of the prototype is shown in **Figure 11**. And the dimension is given accordingly.

3.2.2. Array Design

For one unit we got on average of 238mV. So, it was designed to get 12V on average. For that 11*6 array was designed to get that output. For the exact possible output, we have to make sure that the rectifying circuit is properly designed.

For getting the 12V from the noise barrier 11 by 6 array was designed accordingly. This mainly represents the 66 units of the main prototype attached to gain this noise barrier. The calculation of this noise barrier is given below.

One unit produces 281mV on average. Then 66 unit will produce, $66 \times 238 \times 10^{-3} \text{ mV} = 15.708 \text{ V}$. This voltage goes as input in the rectifying circuit which can be stored or used to run any small devices.

This array was designed also in SolidWorks. Two of the view given below. These two views will show the whole view of the array. And the understanding of the noise barrier and how it will work. The noise barrier is one of the main points of the future work which will be discussed later in the result and discussion chapter.

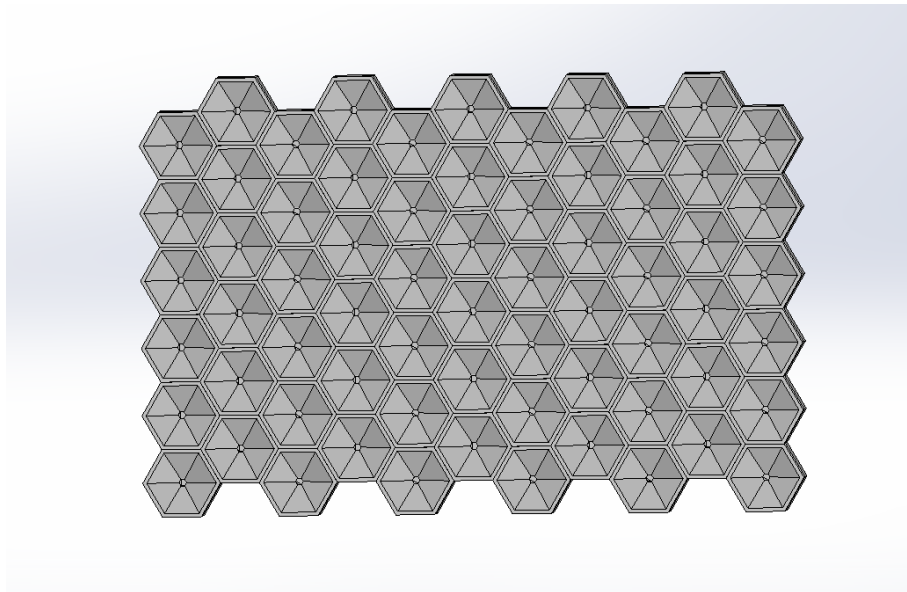


Figure 12. Top View of the array.

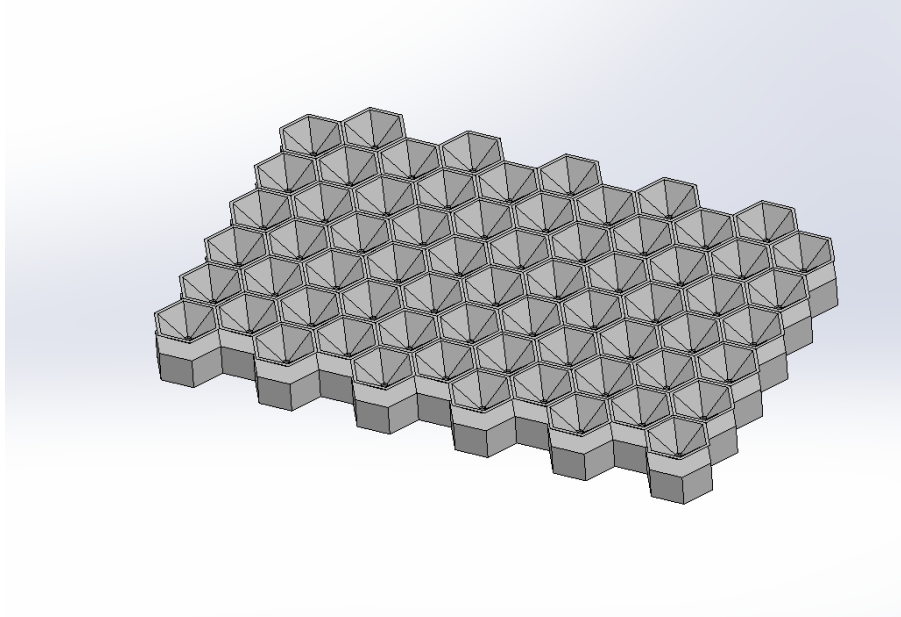


Figure 13. Isometric View of array

Here **Figure 12** and **Figure 13** represent the top view and the isometric view of the 11 by 6 array model which gives a better understanding of the noise barrier.

3.3. 3D Printing Machine

To convert, the CAD model into a physical model, Ultimaker3 was used, which is shown in **Figure 14**. The main CAD file was first converted into STL format to input it to this 3D printer. Polylactic acid (PLA) was the material for this prototype as it is a well-known and easily available material to be found. Around 33 hours were needed to build the prototype. After that, the model was maintained accordingly to be used for further work in our experimental work process.

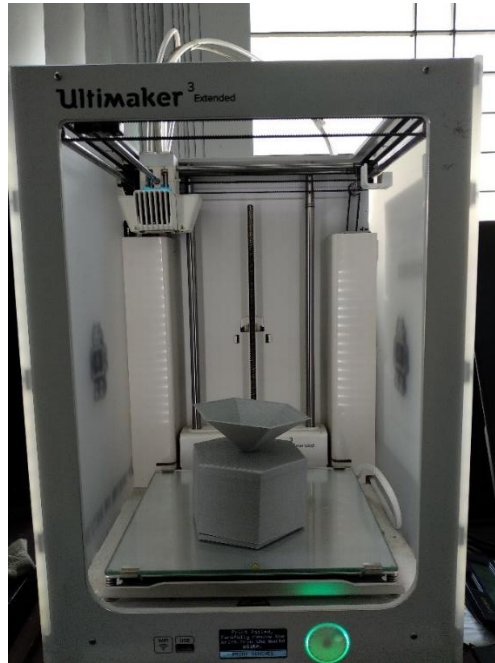


Figure 14. 3D printing machine

3.3.1. 3D Model

For creating the 3D model PLA (Polylactic acid) was used. Based on its easy availability it has been chosen. To achieve the 3D model we have to use the CAD model properly.



Figure 15. Top view of the prototype

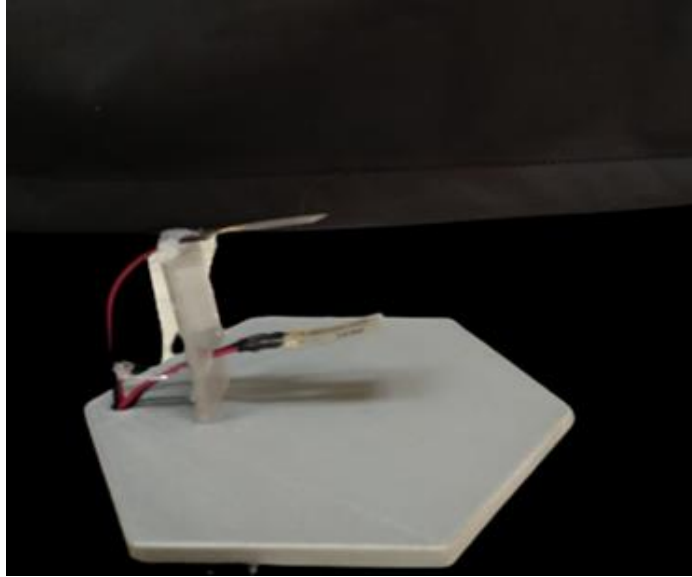


Figure 16. Side view of the prototype

In this top view and the side view, it is seen that the inner part having two films inside. For the experimental setup, these two films are attached to the inner part with the help of the glue gun. It has to be attached carefully so that other impedance from surroundings can not affect the piezoelectric film. As there is so much another factor in the surroundings to be taken care of. Like the sound from surroundings and the direct pressure from the human also.



Figure 17. Front View of prototype

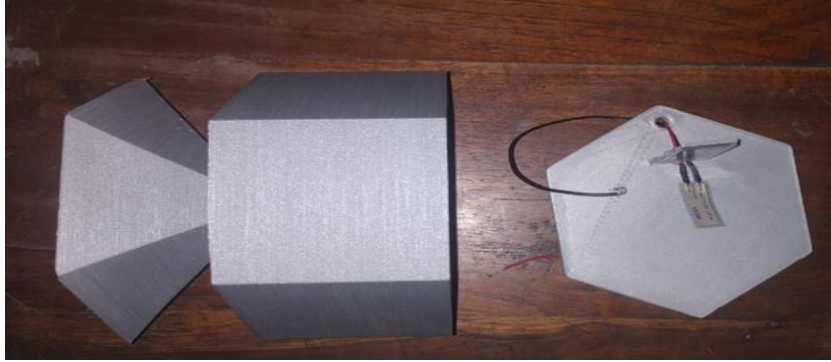


Figure 18. Disassemble View of prototype

Front view of the 3D model produced as the CAD model that was designed earlier. The front view assembled view gives us a clear idea of the prototype itself. Disassemble view of the prototype is also shown here. From this view, the prototype's bottom and top parts can be observed. Low-frequency sound will enter through the top part of the prototype and the sound will create pressure in the piezoelectric film also. The 3D model plays an important role in this experiment. Perfect measurements give us the better result possible. As it's halfway so it has a rectifier have to use the best possible outcome to watch.

3.4. PZT film description



Figure 19. PZT film.

PZT film was used for the experiment which is shown in **Figure 20**. The principal property of these film products meets the substance constraints of Directive 2011/65/EU restricting hazardous substances (RoHS2). The RoHS2 Limited for the absence of mercury, cadmium, hexavalent chromium, PBB, PBDE, lead, DEHP, BBP, DBP, and DIBP above-defined thresholds in these electric equipment products. No of these substances exceeds prohibition thresholds in the products designated as 'Compliant.' CE marked as required by the Directive shall be finished electrical and electronic equipment products. CE may not be marked for the components. Properties of commonly used piezoelectric materials PZT–Lead zirconated titanate are shown in **Table 1**.

Table 1

Properties of commonly used piezoelectric materials PZT–Lead zirconated titanate [42].

Property	Units	PZT
Relative dielectric constant	-	1000–4000
Piezo charge constant d31	pC/N	-600–100
Electromechanical coupling factor	%	30–75
Young’s modulus	10^{10} N/m ²	6–9
Density	kg/m ³	7500–770

Different parameters of the piezoelectric film which was used for the experiment are shown in Table 2. The PZT film part generates more than 10 millivolts per microwave, approximately 60 expanded its product than voltage output of the slate strain gauge. Capacity is proportional to the area and roughly equal to the size of the element.

Table 2

Different parameters of the piezoelectric film which was used for the experiment.

Part Number	1-1002149-0
Film Thickness	28 μ m
Film	.64 (16)
Electrode	.484 (12)
Film	1.63 (41)
Electrode	1.19 (30)
Total Thickness (μ m)	40
Cap (nF)	1.378

The PZT series testers are the simplest type of piezo film sensors, mainly used as flexible dial gauges and touch microphones for vibration or impact detection. These are usable without a lead for such systems that the user needs to make their lead connection. The sensor can be conveniently connected to the dual tape or epoxy board. Lead binding can be accomplished by compressive clamping, crimping, eyelets, conductive epoxy, or low-temperature clamping.

3.5. Experimental details

3.5.1. Components description

3.5.1.1 Function generator

A piece of electronic test equipment or program for generating various types of electrical waveforms over a wide spectrum of frequencies usually constitutes a function generator. The sine, square wave, triangular waves, and sawtooth forms represent some of the most common waveforms generated by the function generator.



Figure 20: Function generator

For this experiment, TEXIO (FG-281) Function Generator was used which is shown in **Figure 21**. In this experiment, a function generator was used to generate a sine wave which was observed by the oscilloscope. The function generator was connected to the power amplifier to generate the signal and amplify the signal also.

3.5.1.2 Oscilloscope

An oscilloscope is a laboratory tool widely used for displaying and analyzing electrical signal waveforms. The unit directly sketches a time graph of the instantaneous signal voltage.

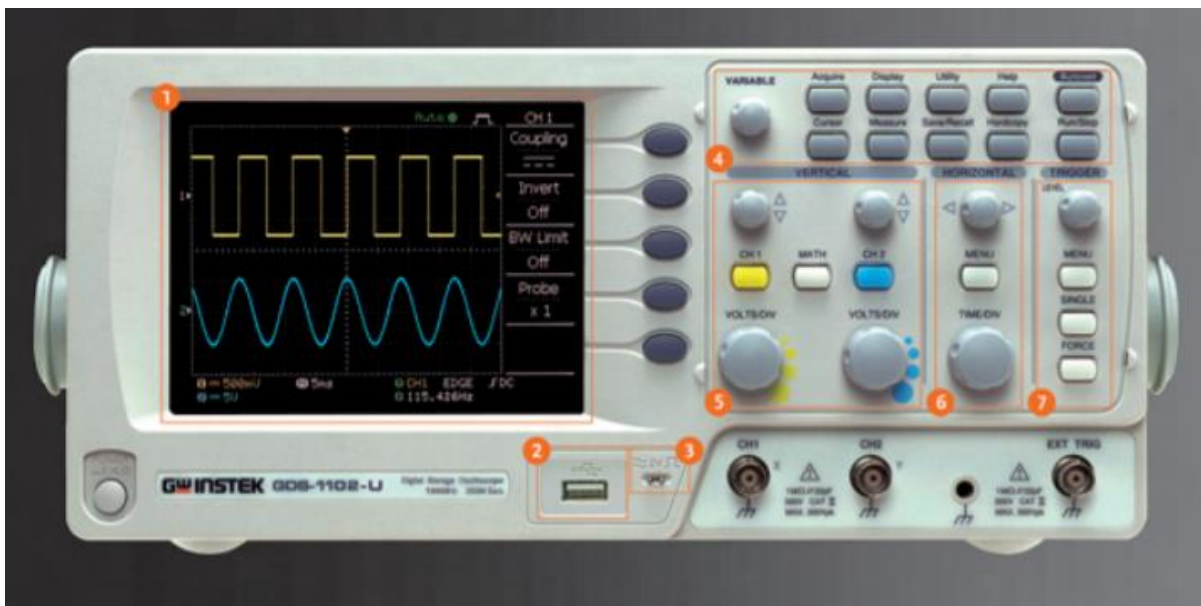


Figure 21: Oscilloscope

For this experiment, Gwinstek (GDS-1102) oscilloscope was used which is shown in **Figure 22**. An oscilloscope was connected to the function generator to observed the wave of the function generator. The function generator produces the sine wave and that connected to the speaker which produces the sound that makes the impedance on the piezoelectric film.

3.5.1.3 Power amplifier

An electronic amplifier is designed to increase the size of a given signal's output. The power of the input signal increases to a degree sufficiently high for driving output unit loads such as speakers, headphones, RF transmitters, etc. A power amplifier is designed to directly drive loads and is used as a final block in the amplifier chain in contrast to current and voltage amplifiers.



Figure 22: Power amplifier

For this experiment, The ModalShop (MODEL 2100E21-400) Power Amplifier was used which is shown in **Figure 23**. The power amplifier amplifies the signal which comes from the function generator. It amplifies by 1.1 and that signal is sent to the speaker and that speaker produces the sound that goes through the prototype and makes the piezoelectric material to produce the electricity.

3.5.1.4. Speaker

Speakers are one of the most popular computer system output instruments. Such speakers are specially made for computers, while others can be connected to a sound system of any kind. Whatever their design, speakers are built to create audio where the listener can hear.



Figure 23: Speaker

For this experiment D7 speaker was used which is shown in **Figure 24**. This speaker captures the sound from the power amplifier and that sound goes through the prototype in the piezoelectric film and that film with the help of sound pressure produces electricity.

3.6. Experimental setup

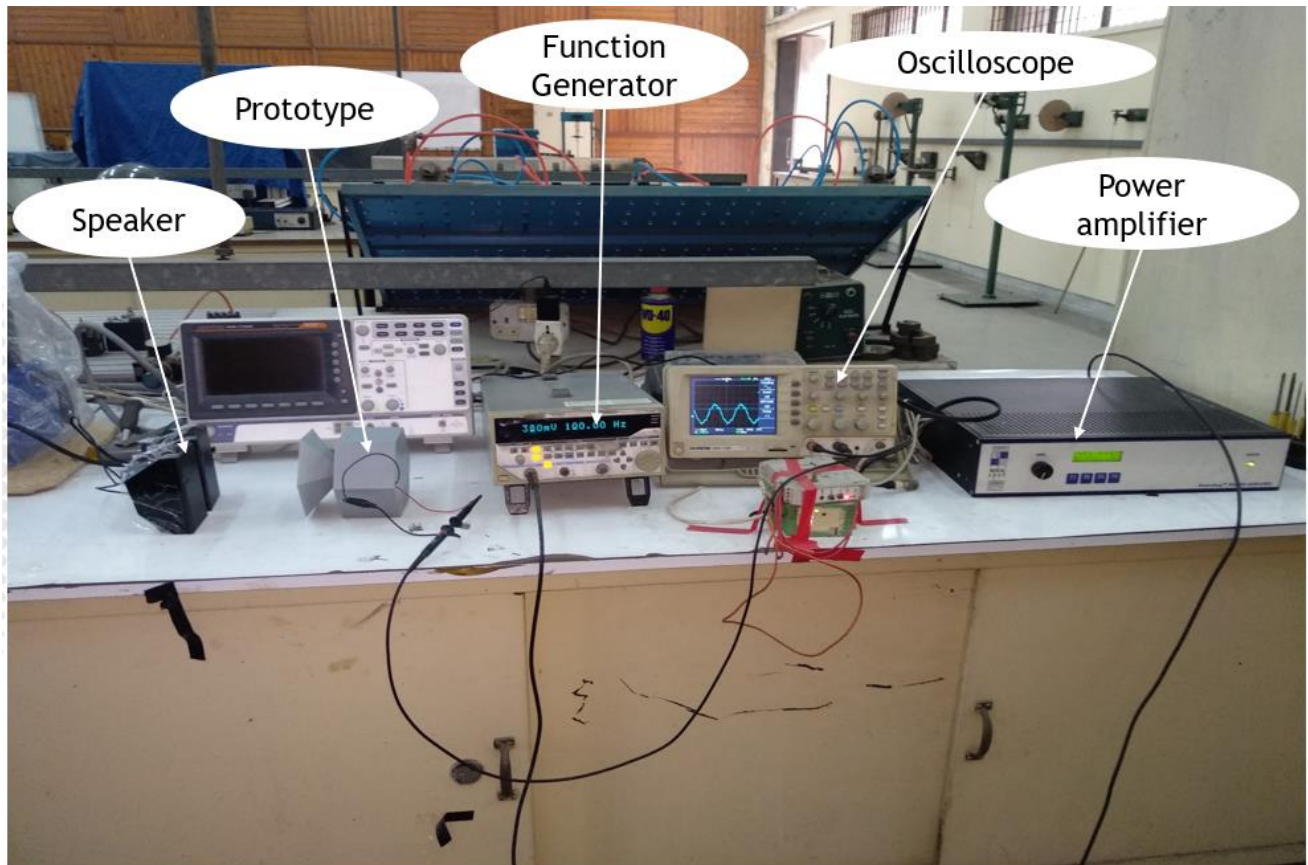


Figure 24. Experimental Setup

For the experimental setup and acquiring data from the experiment components are arranged accordingly which is shown in **Figure 25** . In this arrangement, the power amplifier is connected to the function generator to provide the desired signal response in a definite sine wave produces by the function generator. Then the function generator connects to the oscilloscope to observed the signal which another action was to observe the change in a wave function because of the displacement of the piezoelectric film. Speaker will generate the sound signal that will set on the function generator that sound from the speaker can be controlled by the power amplifier. For the start, the power amplifiers are set to a 1.1 amplify rate. This sound signal will enter the piezoelectric film through a prototype and the sound pressure from the speaker make the impedance on the film that action will make the film displaced from its position and that displacement will generate electricity. After that, the voltage of the film can be measured by the

multimeter and store the data accordingly. The flow diagram of the experimental setup is shown in **Figure 26**.

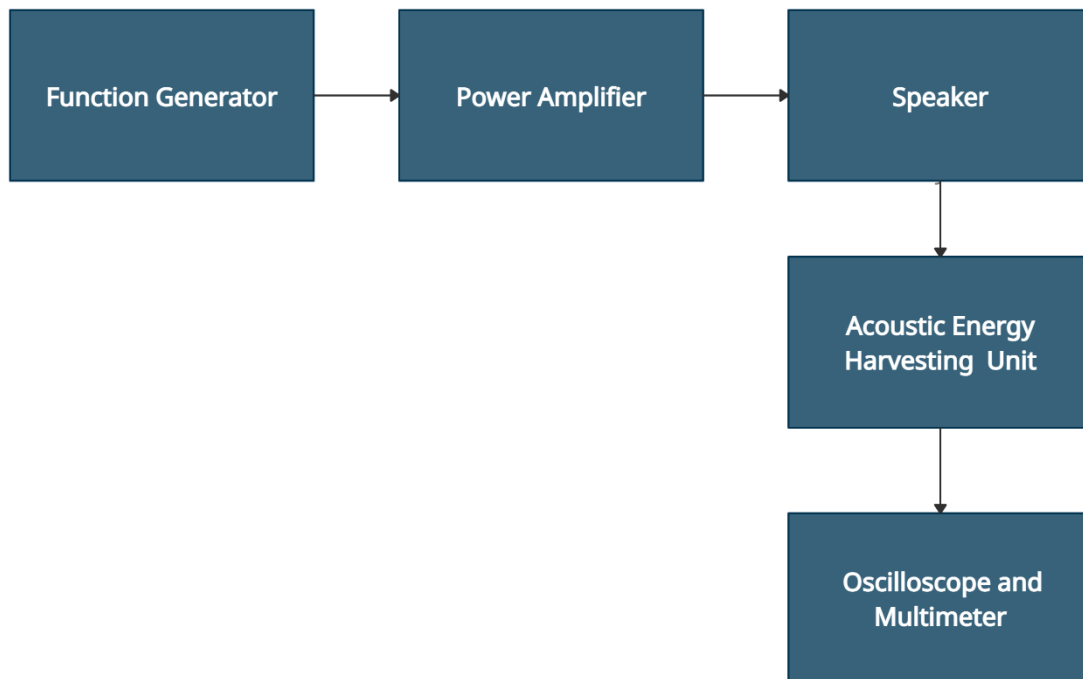


Figure 25. Flow diagram of the experimental setup.

3.7. Boundary Condition

For this experiment, some boundary was set to observe the outcome. These boundary conditions are set based on some arbitrary assumptions. As this is an experimental setup so the main objective there was to observe the output changing based on what was set in the input on the function generator. The spacing between the speaker and prototype was also determine based on the wavelength of each of the speakers.

$$y = y_1 + y_2 \tag{14}$$

This equation of two individual wave intercept with one another makes the superposition wavelength and entering in the prototype.

Spacing was 100mm from the speaker to the prototype. As two of the waves will intercept with one another the spacing have to be accurate.

There are also some boundary conditions on voltage and frequency to observed the output voltage.

Table 3

The boundary conditions between the voltage and frequency

Voltage	Frequency
500mV(fixed)	100Hz-200Hz (variable)
1000mv(fixed)	100Hz-200Hz (variable)
500mV-1.5V(variable)	100Hz(fixed)

3.8. Rectifying circuit simulation

As all the energy harvesting units in the AEHNB are connected in series the voltage from the whole unit gives an unstable current output which can only be used by rectifying it using a voltage regulator. A rectifying circuit is constructed in proteus using 6 Volt and 12 Volt adjustable regulators and other necessary components as shown in the voltage regulator datasheet. The simulation is limited to only charging a small capacitor for short charge and discharge time and lighting a LED. The breakdown voltage of the LED is set to 4 Volts. Although the simulation only lights an LED practical applications of such AEHNB units can be multifarious when supercapacitors are used. The stored energy can be applied to multiple uses, such as monitoring, emergency lights, and sensors. The study of Wang et al. shows the electric circuit for the AEHNB. According to the analysis, a prototype of the AEHNB was physically produced and set in the vicinity of the residential area. When compared with the conventional sound energy harvesting technologies available, the AEHNB can extract the acoustic energy from the high-intensity sound made by running high-speed trains while reducing the noise in the residential area [our main paper]. In the literature [43], at a distance of 25.0m from the high-speed rail centerline, the noise level can reach more than 90 dB in many countries. TGV Reseau in France has a noise level of 97 dB at a speed of 350 km/h [43]. CRH in China has a noise level of 92 dB at a speed of 347 km/h. Considered the closer installation position along HSR, the noise barrier will receive a higher noise level. The rectifying circuit is built-in Proteus 8.0 considering input from an 11 by 6 AEHNB unit or 66 acoustic energy harvesting units.

Figure 27 and **Figure 28** show rectifying circuits for both single and double film configuration and both circuits are similar with minor differences as both circuits implement LM1117DT adjustable voltage regulator. For both circuits, the same model capacitor of 0.01 mF has been used. Only changes in the circuits come down to resistances which have been optimized via trial and error. As can be seen in the figures, the circuit of the double film configuration has a comparatively higher load across the output than the single film configuration. This is obviously due to the difference of input between single and double film energy harvesting units. When the simulation is run the capacitor takes seconds to get charged and the led lights up. Initially, the LED is less bright but gradually the brightness increases and the LED becomes a bright red indicating maximum output. Both circuits contain two current and two voltage probes. One voltage and one current probe read data from before the voltage regulator. The other current and voltage probes are used to read data across the load resistance. These probes are used to generate graphs that visually depict the variation of current and voltage for a period of 11 seconds.

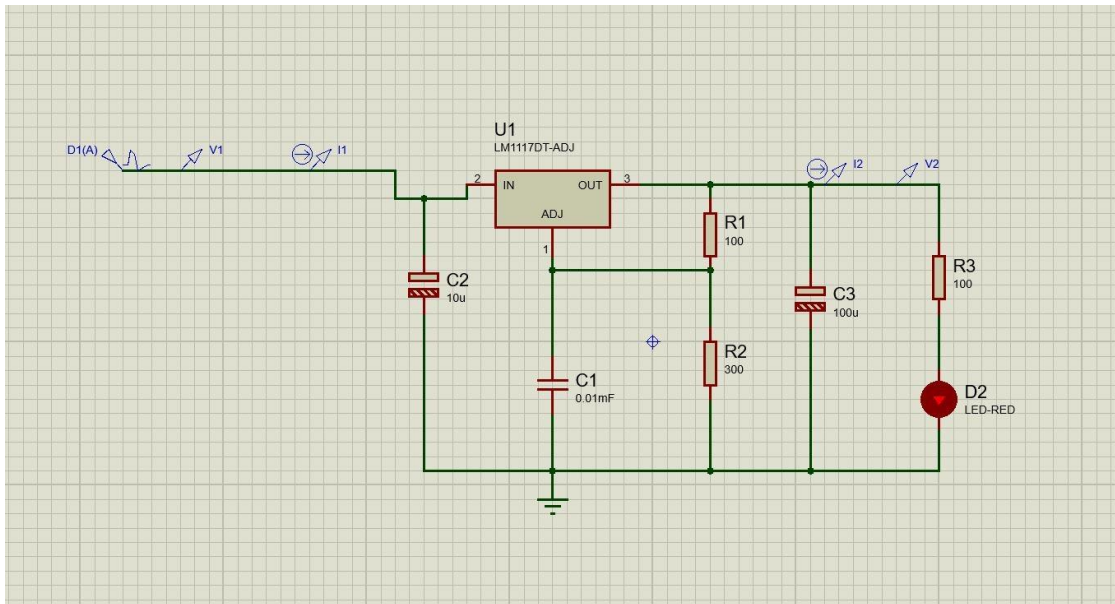


Figure 26. Rectifying circuit considering the single film configuration.

The rectifying circuit in practical applications also work as power modules and store power for later usage. The higher output voltage across the load can be obtained using multiple supercapacitors and transducers. The short charging time of supercapacitors and long discharge time can power up batteries, light up bulbs, charge phones, and laptops, and so on. Even if the rectifying circuit output is limited by the op-amp output saturation voltage, but the final output can be increased to arbitrarily high voltage using multiple stages of voltage multiplier circuit to charge a rechargeable DC battery of higher voltage. In that case, the output current will be reduced and the battery will require more time to be charged.

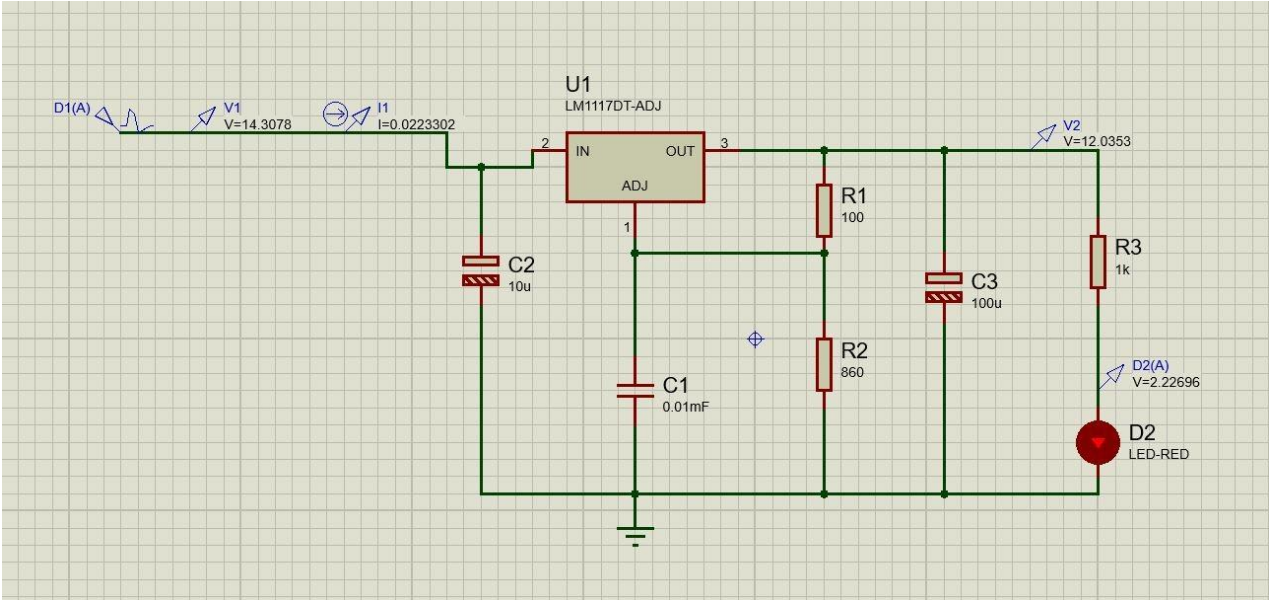


Figure 27. Rectifying circuit considering the double film.

Chapter 4: Results and Discussions

4.1. Experimental results

The acoustic energy travels from two subwoofers and the combined wave travels through the inlet of the resonator and impinges on the piezoelectric films creating excitation. The voltage output from the piezoelectric film terminals is recorded in the oscilloscope and multi-meter for analysis of the energy harvesting unit. However, the place where experimentation was done, was not soundproof and thus background noise cancellation was not an option. Therefore, the experimental setup is placed in the vicinity of the subwoofers to minimize noise and error.

Both the RMS voltage and frequency of the sound wave generated by the function generator are recorded for analysis of the input energy. The function generator generated a sine wave with an amplitude of 2Vpp and the frequency is varied between 100-200 Hz. The incident wave sound pressure level (SPL) has been calculated using the following equation.

$$SPL(dB) = (20 \log_{10} \left(\frac{V_{rms}}{S \times P_{ref}} \right)) \quad (15)$$

Here, the sensitivity of the microphone, $S = 12.6 \text{ mV/Pa}$ [44]. The reference pressure, P_{ref} is taken $20 \text{ } \mu\text{Pa}$ which is the lowest threshold for the human hearing with an SPL of 0 dB. The SPL ranges from 125.95 dB to 135.49 dB.

The testing of the piezoelectric energy harvester was started without the Helmholtz resonator at first to understand the importance of the single degree of freedom (SDOF) system. The output voltage from the terminals of a single film was recorded under varying conditions of input voltage and frequency in the function generator. **Figure 29** depicts the variation of output voltage with increasing input voltage in function generator from 500 mV to 1500 mV with a step size of 100 mV. Without the resonator, the acoustic energy harvesting pattern is unpredictable and irregular. The output voltage increases up to around 900 mV input voltage. The peak output here is 107.7 mV. Then for increasing input voltage the output significantly drops and again rises at 1300 mV input. For the further rise in input voltage, the output falls sharply. This kind of irregular behavior at high input voltage might happen due to the intervention of background noise with subwoofer sound waves. Irregular behavior in output voltage is also seen in the plot of output voltage vs

frequency at 500 mV constant input voltage. The frequency is set from 100 Hz to 200 Hz with a step size of 10 Hz. The overall plot shows increasing output voltage with increasing frequency which should be the normal trend but isn't free of irregularities at certain frequencies. **Figure 30** shows the relation between the output voltage and input frequency for a single film without any resonator at a constant 500 mV input voltage set in the function generator. The highest output voltage is 120 mV for 200 Hz input in the function generator.

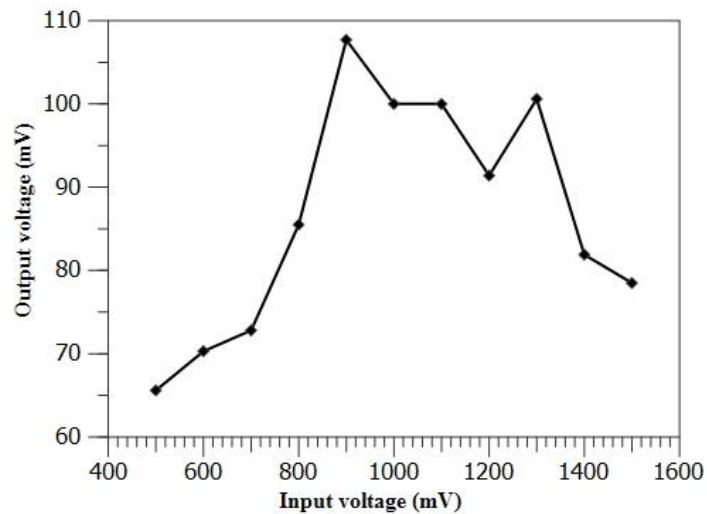


Figure 28. Input voltage vs. Output voltage for a single film without the resonator.

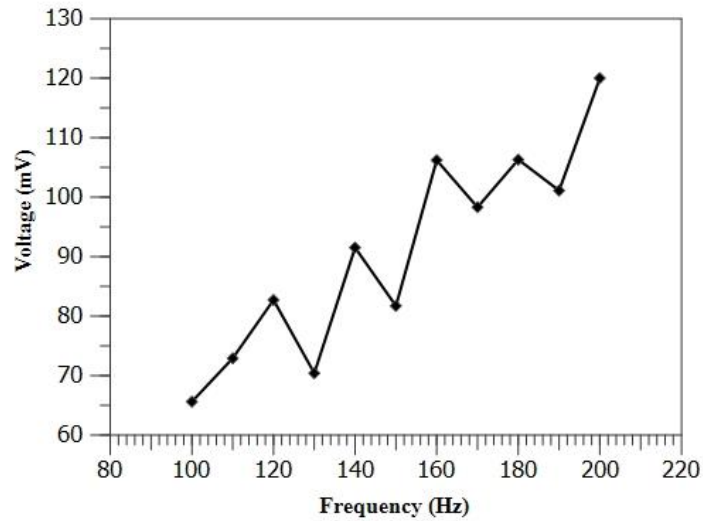


Figure 29. Frequency vs. Voltage for a single film without the resonator.

Then the experiment is done with a resonator and significant improvements in the output voltage regularity are seen. **Figure 31** shows the plot of output voltage with increasing input voltage at a constant frequency of 100 Hz for both single and double film configuration and as expected, double film configuration brings out far better voltage output at the terminals. The highest output voltage achieved by single film configuration of acoustic energy harvester is 201.3 mV at 1500 mV input voltage. Whereas, the highest output of the double film configuration is 208.2 at only 1100 mV input voltage. The advantage of double film is truly understood by the graph in the figure. It is clear that at any certain input level, double film configuration gives the output as high as 200% of single film configuration.

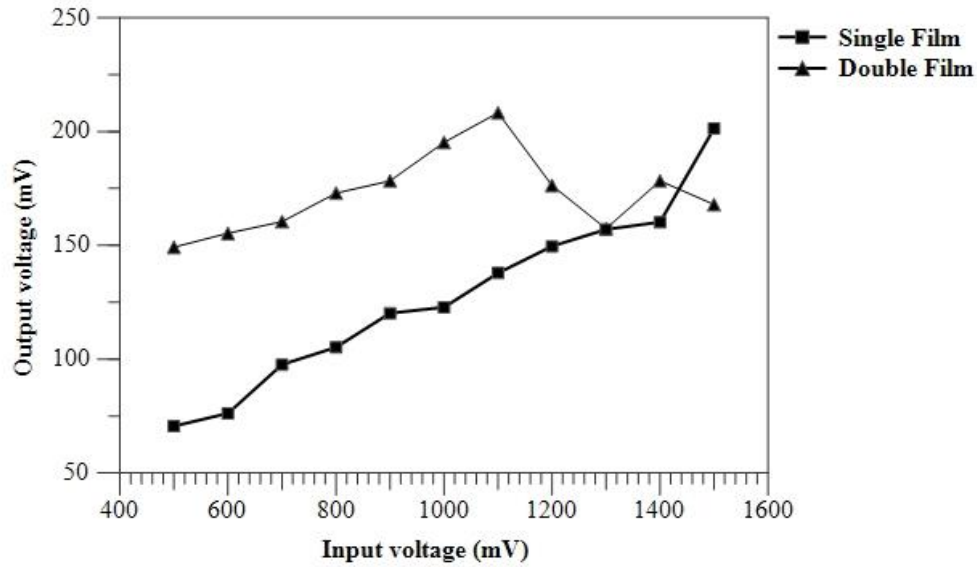


Figure 30. Input vs. output Voltage at 100 Hz for both single and double film configuration with a resonator.

One point of concern is the decline in the output voltage of double film units after 1100 mV input. This again might have happened due to background noise in the experimentation space. **Figure 32** depicts the difference between single and double film units in energy harvesting capacity more clearly. The figure shows the plot of output voltage with frequency and compares the output of single and double film configurations at a constant 500 mV input voltage set in the function generator. At 170 Hz input, the double film configuration gives 237.6 mV output whereas the single film unit gives 80.2 mV only.

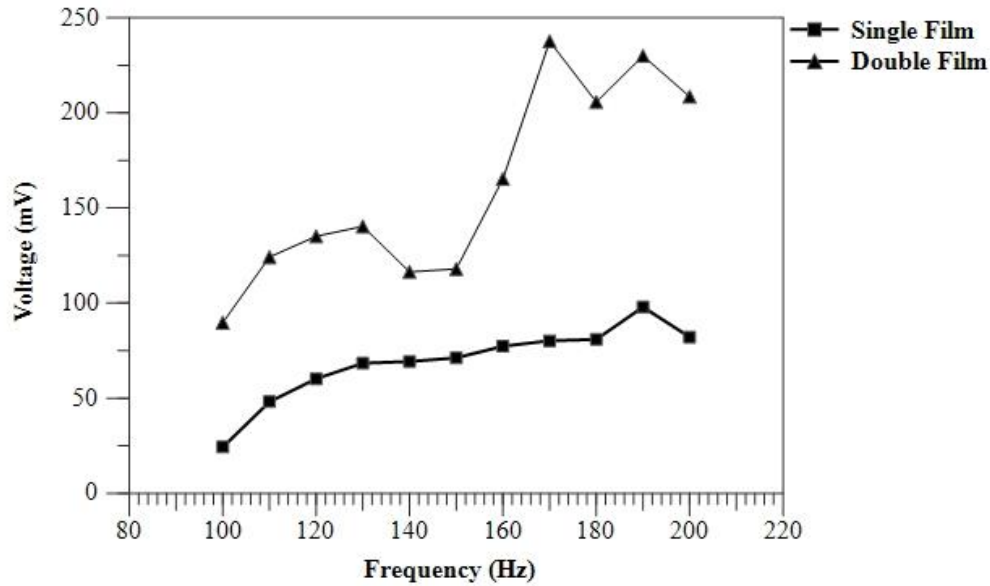


Figure 31. Output voltage vs frequency at 500 mV input voltage for both single and double film configuration with a resonator

Figure 33 depicts a similar plot of output voltage vs. frequency but at a constant 1000 mV input voltage set in the function generator. The visual depiction of the output voltage shows a similar trend as in the previous figure. For instance, at an input frequency of 130 Hz, the double film unit gives 166.4 mV output voltage whereas the single film unit gives only 106.7 mV output only. The analysis of output voltage with increasing input voltage or frequency clearly shows step by step that Helmholtz resonator can give better acoustic impedance on the piezoelectric film and a double film configuration is better in capacity than a single film configuration and further addition of films might also be possible for further improvements in energy harvesting technologies.

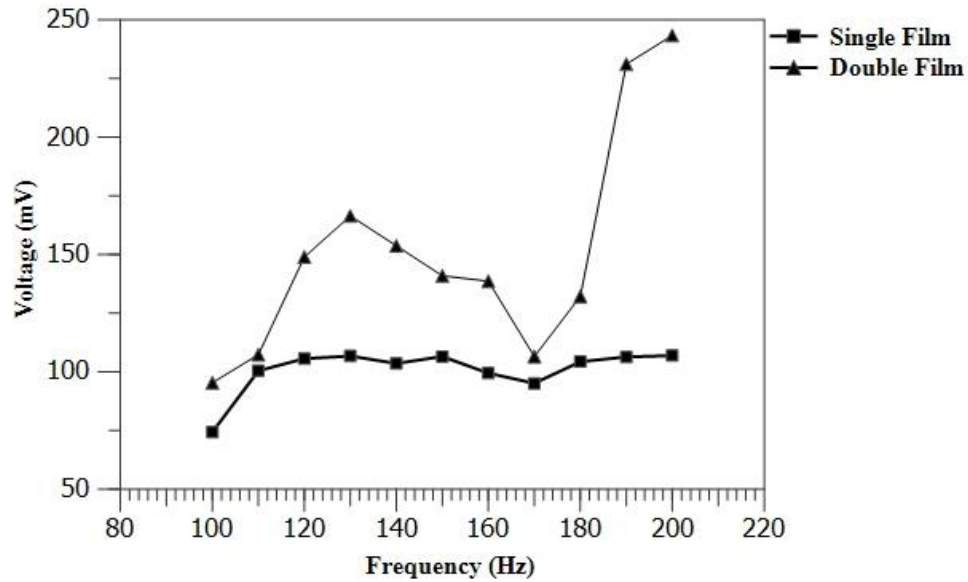


Figure 32. Output voltage vs frequency at 1000 mV input voltage for both single and double film configuration with a resonator.

Figure 34 and **Figure 35** depict the change in output voltage with increasing input SPL. In figure-30, the single film configuration shows a good trend in the graph, and the highest output is obtained at the highest input sound pressure level (SPL). **Figure-34** shows the trend of output voltage change with increasing SPL. The output voltage increases up to around 133 dB and then a sharp fall is observed. This irregularity is observed several times in the results due to unfavorable experimentation space with lots of noise and unregulated sound sources.

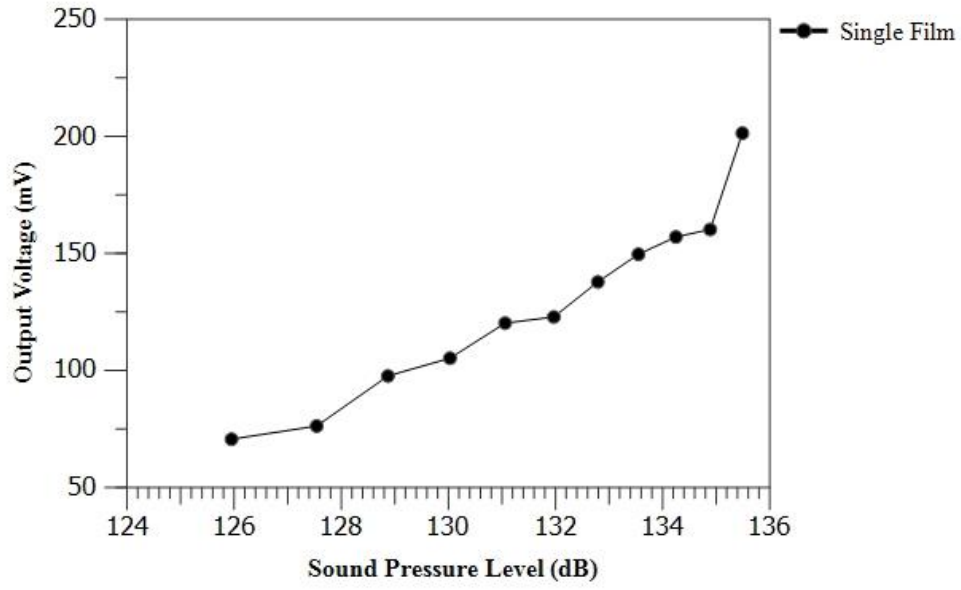


Figure 33. Output voltage vs sound pressure level for single film configuration.

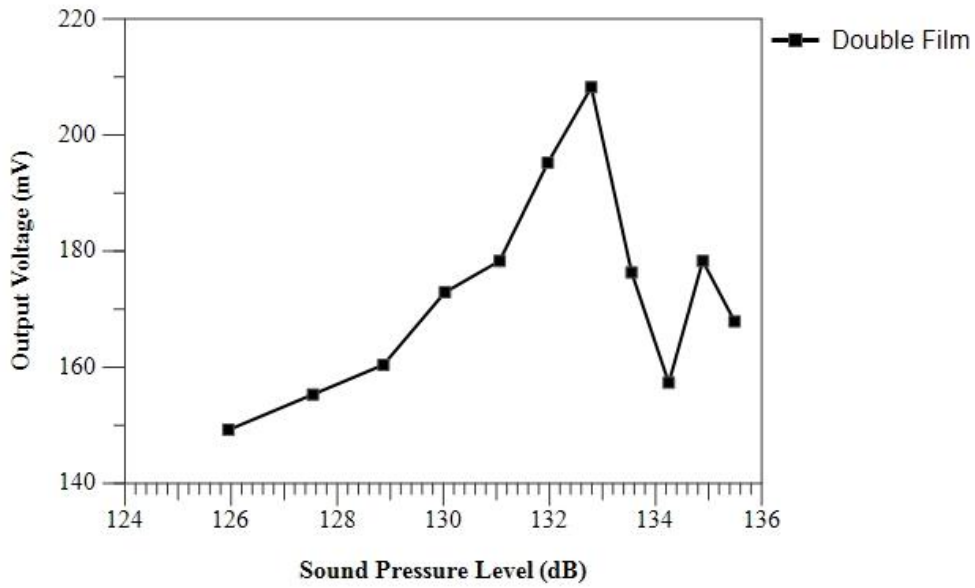


Figure 34. Output voltage vs sound pressure level for single film configuration.

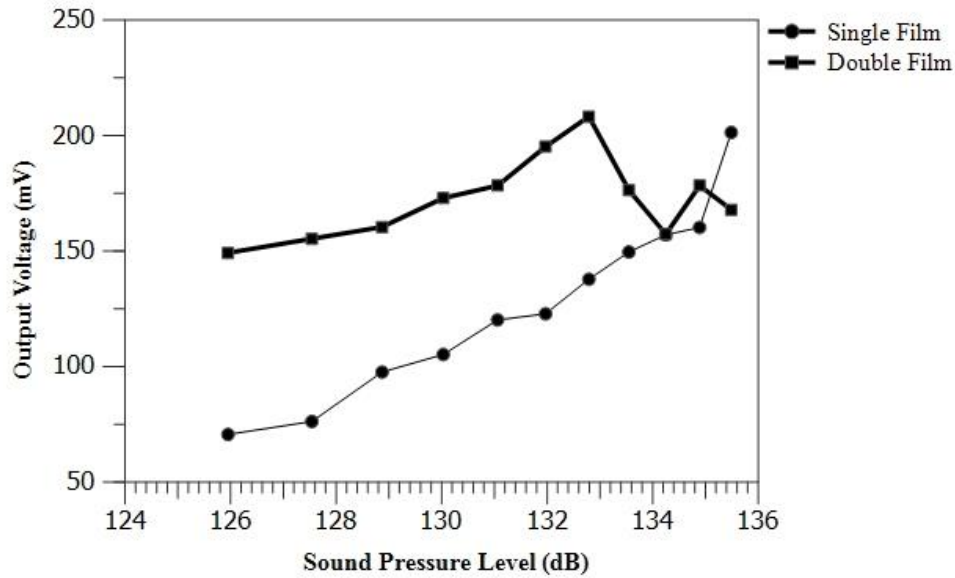


Figure 35. Output voltage vs sound pressure level for single and double film configuration.

Both the results are compared in **Figure 36** and naturally, the performance of the double film configuration is better up to 133 dB after which irregularities in the output come into play.

4.2. Simulation results

The rectifying circuit is shown previously which has been simulated in Proteus 8.0 also gives us some current and voltage data which must be analyzed to understand the level of power that can be generated by the proposed noise barrier units. Each graph here depicts the variation of current or voltage with time. The time set here is 11 seconds. This is because a very small capacitor has been utilized in the rectifying circuit for the ease of simulation.

Figure 37 shows the variation of total circuit current and current at the final load with time and we can see that the load current is slightly less than the total circuit current but shows the same pattern of alteration with time. This is the current from the noise barrier unit considering single film configuration. **Figure 38** depicts the variation of total input voltage and load voltage with time and we can see that after 6 seconds the voltage at the load is stabilized at 5 volts.



Figure 36. Input and load current vs time plot for one film AEHNB model.



Figure 37. Input and load voltage vs time for one film AEHNB model.

Figure 39 and **Figure 40** depict the variation of current and voltage in the rectifying circuit for double film noise barriers. As shown in **Figure 39**, the total current and load current follow the same pattern of variation and stabilizes after 7.5 seconds of starting the simulation. The current at stable state at the load is 10 mA and the total current is on the upper side of 20 mA.

The voltage from the noise barrier and the load voltage plot with time shows how the input voltage is always unstable throughout the cycle. But the load voltage stabilizes after 7.5 seconds of starting the simulation at 12.2 volts as a 12-volt voltage regulator is used. The voltage regulator used in

both the circuits is adjustable and the voltage and current probes show that the circuit can run small devices and can charge up even supercapacitors for better charging and discharging.

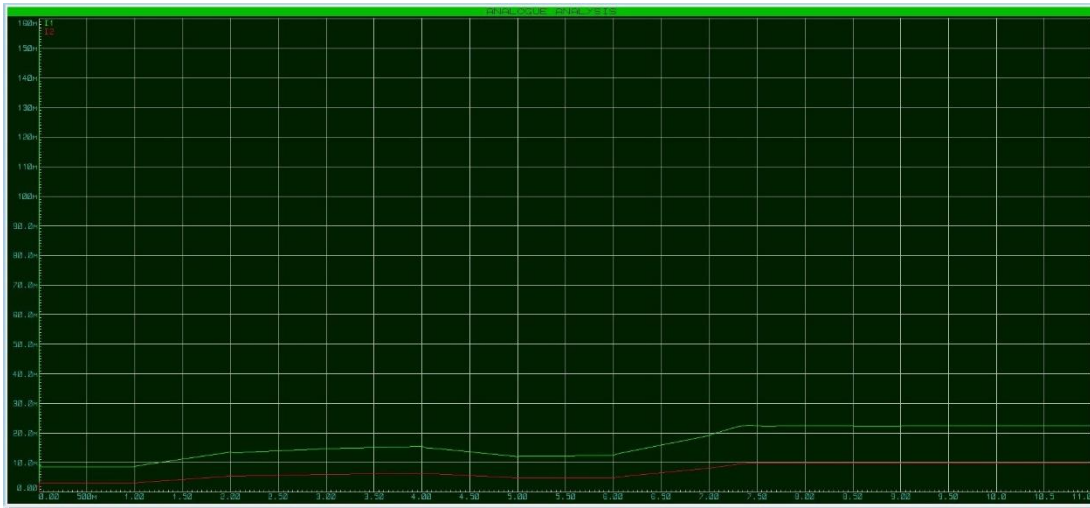


Figure 38. Input and load current vs time plot for two films AEHNB model.



Figure 39. Input and load voltage vs time for two films AEHNB model.

The total output power of the double film noise barrier made with 66 units is found to be 268.8 mW. So each energy harvesting unit is producing 4.07 mW power in the rectifying circuit. The total power output of a single film noise barrier is 136.77 mW and thus the power output of a single unit is 2.07 mW. This power can be stored using a power module similar to this rectifying circuit. The noise barrier units can be used in metro-rail projects that go through residential areas and even small or big factories which generate loud noise.

The results obtained in both experiments and simulation are not free of error due to environmental and other effects. Some discussions on the results are as follows.

- The honeycomb structure can be further improved by better 3D printing technology so that the finishing in the neck and edge areas are finer and the acoustic behavior and transmission improve.
- The Helmholtz resonator structure can be geometrically analyzed to get a better response on the PZT film and thus better output.
- The experiment should be done in a noise-free lab where background noise cancellation is possible and thus no interventions from outside noise are possible.

Chapter 5: Future scope and Conclusion

In this study, a renewable low-frequency acoustic energy harvesting prototype is reasonably, systematically, and successfully developed for industrial areas and Dhaka metro rail, especially in residential areas where noise pollution is high. The proposed system provides a practical solution for both low-frequency sound absorption by using huge arrays of barriers and generation of the electricity to power up low power consuming devices like automobile lights, factory lights, and low power electronic devices. The purposes of noise reduction and electricity generation are achieved by the proposed system through the transformation of sound energy to electricity using a PZT (Lead Zirconate Titanate) film in a Helmholtz resonator structure to provide a better acoustic effect on the PZT film.

Helmholtz structure with better acoustic impedance on PZT film may yield better results in the future. Future researchers can work on developing the film structure and positioning in the resonator. More controlled sound energy input and addition of diaphragm can yield better results can help in getting more accurate results. Small and big power plants and industries which produce loud noise can also utilize this technology to save electricity and reduce the noise level which can be helpful for the workers and residents of the industrial areas.

References

- [1] P. Glynne-Jones, M. J. Tudor, S. P. Beeby, and N. M. White, “An electromagnetic, vibration-powered generator for intelligent sensor systems,” *Sensors Actuators, A Phys.*, vol. 110, no. 1–3, pp. 344–349, 2004.
- [2] S. B. Horowitz, M. Sheplak, L. N. Cattafesta, and T. Nishida, “A MEMS acoustic energy harvester,” *J. Micromechanics Microengineering*, vol. 16, no. 9, 2006.
- [3] F. Liu, S. Horowitz, T. Nishida, L. Cattafesta, and M. Sheplak, “A multiple degree of freedom electromechanical Helmholtz resonator,” *J. Acoust. Soc. Am.*, vol. 122, no. 1, pp. 291–301, 2007.
- [4] M. Ferrari, V. Ferrari, M. Guizzetti, D. Marioli, and A. Taroni, “Piezoelectric multifrequency energy converter for power harvesting in autonomous microsystems,” *Sensors Actuators, A Phys.*, vol. 142, no. 1, pp. 329–335, 2008.
- [5] L. Y. Wu, L. W. Chen, and C. M. Liu, “Acoustic energy harvesting using resonant cavity of a sonic crystal,” *Appl. Phys. Lett.*, vol. 95, no. 1, pp. 2007–2010, 2009.
- [6] M. Lallart, D. Guyomar, C. Richard, and L. Petit, “Nonlinear optimization of acoustic energy harvesting using piezoelectric devices,” *J. Acoust. Soc. Am.*, vol. 128, no. 5, pp. 2739–2748, 2010.
- [7] D. Vatansever, R. L. Hadimani, T. Shah, and E. Siores, “An investigation of energy harvesting from renewable sources with PVDF and PZT,” *Smart Mater. Struct.*, vol. 20, no. 5, 2011.
- [8] B. Li and J. H. You, “Harvesting ambient acoustic energy using acoustic resonators,” *Proc. Meet. Acoust.*, vol. 12, no. May, pp. 1–8, 2011.
- [9] B. Li, A. J. Laviage, J. H. You, and Y. J. Kim, “Harvesting low-frequency acoustic energy using multiple PVDF beam arrays in quarter-wavelength acoustic resonator,” *Appl. Acoust.*, vol. 74, no. 11, pp. 1271–1278, 2013.
- [10] B. Li, J. H. You, and Y. J. Kim, “Low frequency acoustic energy harvesting using PZT piezoelectric plates in a straight tube resonator,” *Smart Mater. Struct.*, vol. 22, no. 5, 2013.

- [11] Z. R. Abrams, A. Niv, and X. Zhang, "Solar energy enhancement using down-converting particles: A rigorous approach," *J. Appl. Phys.*, vol. 109, no. 11, 2011.
- [12] V. J. Ovejas and A. Cuadras, "Multimodal piezoelectric wind energy harvesters," *Smart Mater. Struct.*, vol. 20, no. 8, 2011.
- [13] B. J. Hansen, Y. Liu, R. Yang, and Z. L. Wang, "Hybrid nanogenerator for concurrently harvesting biomechanical and biochemical energy," *ACS Nano*, vol. 4, no. 7, pp. 3647–3652, 2010.
- [14] S. H. Kim *et al.*, "An electromagnetic energy scavenger from direct airflow," *J. Micromechanics Microengineering*, vol. 19, no. 9, 2009.
- [15] S. E. Jo, M. S. Kim, and Y. J. Kim, "A resonant frequency switching scheme of a cantilever based on polyvinylidene fluoride for vibration energy harvesting," *Smart Mater. Struct.*, vol. 21, no. 1, 2012.
- [16] F. Liu *et al.*, "Acoustic energy harvesting using an electromechanical Helmholtz resonator," *J. Acoust. Soc. Am.*, vol. 123, no. 4, pp. 1983–1990, 2008.
- [17] Z. Zhang, X. Zhang, Y. Rasim, C. Wang, B. Du, and Y. Yuan, "Design, modelling and practical tests on a high-voltage kinetic energy harvesting (EH) system for a renewable road tunnel based on linear alternators," *Appl. Energy*, vol. 164, no. September 2015, pp. 152–161, 2016.
- [18] Z. Zhang *et al.*, "A high-efficiency energy regenerative shock absorber using supercapacitors for renewable energy applications in range extended electric vehicle," *Appl. Energy*, vol. 178, pp. 177–188, 2016.
- [19] H. Wang, A. Jasim, and X. Chen, "Energy harvesting technologies in roadway and bridge for different applications – A comprehensive review," *Appl. Energy*, vol. 212, no. August 2017, pp. 1083–1094, 2018.
- [20] S. Orrego *et al.*, "Harvesting ambient wind energy with an inverted piezoelectric flag," *Appl. Energy*, vol. 194, pp. 212–222, 2017.
- [21] H. Vocca, I. Neri, F. Travasso, and L. Gammaitoni, "Kinetic energy harvesting with bistable

- oscillators,” *Appl. Energy*, vol. 97, pp. 771–776, 2012.
- [22] X. Zhang, Z. Zhang, H. Pan, W. Salman, Y. Yuan, and Y. Liu, “A portable high-efficiency electromagnetic energy harvesting system using supercapacitors for renewable energy applications in railroads,” *ENERGY Convers. Manag.*, vol. 118, pp. 287–294, 2016.
- [23] H. Roshani, S. Dessouky, A. Montoya, and A. T. Papagiannakis, “Energy harvesting from asphalt pavement roadways vehicle-induced stresses : A feasibility study,” *Appl. Energy*, vol. 182, pp. 210–218, 2016.
- [24] N. Fondevilla, C. Serre, M. C. Acero, E. Cabruja, H. Campanella, and J. Esteve, “Electromagnetic Harvester Device for Scavenging Ambient Mechanical Energy with Slow , Variable , and Randomness Nature,” no. May, pp. 1–5, 2011.
- [25] Ö. Zorlu, E. T. Topal, and H. KÜlah, “A Vibration-Based Electromagnetic Energy Harvester Using Mechanical Frequency Up-Conversion Method,” vol. 11, no. 2, pp. 481–488, 2011.
- [26] J. Granstrom, J. Feenstra, and H. A. Sodano, “harvesting A review of power harvesting using piezoelectric materials (2003 – 2006),” 2006.
- [27] B. Li and Y. Kim, “IMECE2012-86989,” pp. 1–7, 2016.
- [28] Q. S. Resonator, B. Li, and J. H. You, “Simulation of Acoustic Energy Harvesting Using Piezoelectric Plates in a Simulation of Acoustic Energy Harvesting Using Piezoelectric Plates in a Quarter-wavelength Straight-tube Resonator,” no. September, 2015.
- [29] H. Abdelmoula, N. Sharpes, A. Abdelkefi, H. Lee, and S. Priya, “Low-frequency Zigzag energy harvesters operating in torsion-dominant mode,” *Appl. Energy*, vol. 204, pp. 413–419, 2017.
- [30] M. Guan and W. H. Liao, “Design and analysis of a piezoelectric energy harvester for rotational motion system,” *Energy Convers. Manag.*, vol. 111, pp. 239–244, 2016.
- [31] M. A. Pillai and E. Deenadayalan, “A review of acoustic energy harvesting,” *Int. J. Precis. Eng. Manuf.*, vol. 15, no. 5, pp. 949–965, 2014.
- [32] Z. Zhou, W. Qin, and P. Zhu, “Harvesting acoustic energy by coherence resonance of a bi-stable piezoelectric harvester,” *Energy*, vol. 126, pp. 527–534, 2017.

- [33] Z. Hu, C. Yang, and L. Cheng, “Acoustic resonator tuning strategies for the narrowband noise control in an enclosure,” *Appl. Acoust.*, vol. 134, no. December 2017, pp. 88–96, 2018.
- [34] M. Yuan, Z. Cao, J. Luo, J. Zhang, and C. Chang, “An efficient low-frequency acoustic energy harvester,” *Sensors Actuators, A Phys.*, vol. 264, pp. 84–89, 2017.
- [35] S. Noh, H. Lee, and B. Choi, “A study on the acoustic energy harvesting with Helmholtz resonator and piezoelectric cantilevers,” *Int. J. Precis. Eng. Manuf.*, vol. 14, no. 9, pp. 1629–1635, 2013.
- [36] C. B. Williams and R. B. Yates, “Analysis of a micro-electric generator for microsystems,” *Sensors Actuators, A Phys.*, vol. 52, no. 1–3, pp. 8–11, 1996.
- [37] H. Zhao *et al.*, “Dual-Tube Helmholtz Resonator-Based Triboelectric Nanogenerator for Highly Efficient Harvesting of Acoustic Energy,” *Adv. Energy Mater.*, vol. 9, no. 46, pp. 1–10, 2019.
- [38] A. Ballato, “Dynamic Admittance Matrix of Piezoelectric Cantilever Bimorphs,” *J. Microelectromechanical Syst.*, vol. 3, no. 3, pp. 105–112, 1994.
- [39] S. Roundy and P. K. Wright, “A piezoelectric vibration based generator for wireless electronics,” *Smart Mater. Struct.*, vol. 13, no. 5, pp. 1131–1142, 2004.
- [40] Leonard Meirovitch, “Elements of Vibration Analysis,” *McGraw-Hill*. 1975.
- [41] Y. Wang *et al.*, “A renewable low-frequency acoustic energy harvesting noise barrier for high-speed railways using a Helmholtz resonator and a PVDF film,” *Appl. Energy*, vol. 230, no. April, pp. 52–61, 2018.
- [42] О. Р. Ш. И. В. И. О.В.Ковалишина, “Опыт аудита обеспечения качества и безопасности медицинской деятельности в медицинской организации по разделу «Эпидемиологическая безопасность» No Title,” *Вестник Росздравнадзора*, vol. 4, no. May, pp. 9–15, 2017.
- [43] R. T. Sataloff, M. M. Johns, and K. M. Kost, *No 主観的健康感を中心とした在宅高齢者における健康関連指標に関する共分散構造分析Title.*
- [44] F. U. Khan and I. Izhar, “Electromagnetic-based acoustic energy harvester,” *2013 16th Int.*

Multi Top. Conf. INMIC 2013, pp. 125–130, 2013.